

SUPPORTING INFORMATION

Spin State Chemistry: modulation of ligand pKa by spin state switching in a [2×2] iron(II) grid-type complex

Sébastien Dhers,^a Abhishake Mondal,^{b,c,d} David Aguilà,^{b,c} Juan Ramírez,^a Sergi Vela,^e Pierre Dechambenoit,^{b,c} Mathieu Rouzières,^{b,c} Jonathan R. Nitschke,^{a,f} Rodolphe Clérac^{b,c*} and Jean-Marie Lehn^{a*}

^a *Laboratoire de Chimie Supramoléculaire, ISIS, Université de Strasbourg, 8 Allée Gaspard Monge, 67000 Strasbourg, France. e-mail: lehn@unistra.fr*

^b *CNRS, CRPP, UMR5031, F-33600 Pessac, France. e-mail: clerac@crpp-bordeaux.cnrs.fr*

^c *Univ. Bordeaux, CRPP, UMR5031, F-33600 Pessac, France*

^d *Solid State and Structural Chemistry Unit, Indian Institute of Science, C.V. Raman Road, Bangalore-560012, India.*

^e *Laboratoire de Chimie Quantique, UMR 7177 CNRS-Université de Strasbourg, 1 rue Blaise Pascal, 67008 Strasbourg, France.*

^f *Department of Chemistry, University of Cambridge, CB2 1EW, UK.*

Materials and general methods.

Single Crystal structural data were collected on a Bruker Apex-II CCD Quasar diffractometer using graphite-collimated Mo K α radiation ($\lambda = 0.71073 \text{ \AA}$), except for $[\text{Zn}_4(\text{H}_2\text{L})_4](\text{BF}_4)_8 \cdot 8\text{MeCN}$ (**Zn-8H**) which was collected on a Bruker APEX II DUO Kappa-CCD diffractometer using Cu-K α radiation ($\lambda = 1.54178 \text{ \AA}$). The program SAINT was used to integrate the data, which was thereafter corrected using SADABS.^[1a] The structure was solved using direct methods and refined by a full-matrix least-squares method on F^2 using SHELXL-2014.^[1b] Hydrogen atoms were found in difference maps and subsequently placed at calculated positions using suitable riding models with isotropic displacement parameters derived from their carrier atoms. Non-hydrogen atoms were refined with anisotropic displacement parameters. Additional information about the refinement (constraints/restraints, modelization of disorders and SQUEEZE^[1c] procedure) can be found in the `_refine_special_details` in the cif files.

Magnetic susceptibility measurements were obtained with the use of MPMS-XL Quantum Design SQUID magnetometer. This magnetometer works between 1.8 and 400 K for *dc* applied fields ranging from -7 to 7 T (MPMS-XL). Measurements were performed on polycrystalline solvated samples of 17.26, 10.54 and 1.44 mg, for **Fe-8H**, **Fe-6H** and **Fe-4H** respectively, introduced in a polyethylene bag ($3 \times 0.5 \times 0.02 \text{ cm}$; typically 15-30 mg). *M* versus *H* measurements has been performed at 100 K to check for ferromagnetic impurities which have been found absent. The magnetic data were corrected for the sample holder and diamagnetic contributions.

Elemental analyses for C, H and N were performed on a Perkin-Elmer 240Q elemental analyzer. **Mass spectrometry** spectra were recorded on a Thermo Scientific Exactive Plus EMR in positive ion mode (capillary temperature: 150 °C; spray voltage: 3.6 kV). The ESI-MS spectra were performed on a Finnigan LCQ ADVANTAGE MAX and the data were collected in positive ion mode. **FT-IR spectra** ($4000\text{--}400 \text{ cm}^{-1}$) were measured as Nujol mulls placed between KBr plates on a Bruker Tensor 27 spectrophotometer. **UV-vis experiments** were performed on a Varian Cary 3 with 1cm quartz cuvettes. **NMR spectra** were recorded on Bruker Advance III plus 400 (400.34 MHz for ^1H and 100.67 MHz for ^{13}C) NMR spectrometers. All the collected spectra were referenced on residual solvent signal according to Nudelman and co-workers,^[2] 1.94 ppm for acetonitrile, 7.26 ppm for chloroform. Deuterated solvents were purchased from Euriso-TOP and used after purification on basic alumina and drying over molecular sieves.

Solvents and reagents were purchased from Sigma-Aldrich and Alfa Aesar, and were used without further purification. Ligand H₂L was synthesized according to the literature procedure.^[3]

Experimental part

It is important to note that grids **Fe-8H** to **Fe-4H** are soluble in CD₃CN but further deprotonated grids (**Fe-3H** to **Fe-0H**) are extremely insoluble in CD₃CN but are soluble in CDCl₃. DMSO also solubilizes all the protonated or deprotonated forms of the grid complexes. Nevertheless, no crystals or crystal structure other than the aforementioned could be obtained, even using CDCl₃ and DMSO. Note that the same trend in solubility is observed for Zn grids. For paramagnetic ¹H NMR of the **Fe-nH** complexes, no integral value is given as the spectra are too broad and there is too much exchange present (**Fe-6H** could not be reported due to extremely broad signals). Therefore, the values are given, when given, as an indication. Elemental analysis for **Fe-nH** has been done on dry samples, due to rapid loss of solvent.

[Fe₄(H₂L)₄](BF₄)₈·6MeCN (Fe-8H). 39.5 mg (0.1 mmol) of ligand H₂L and 37.1 mg (0.11 mmol) of Fe(BF₄)₂·6H₂O were dissolved in 6 mL MeCN under argon. After stirring for 10 minutes, 0.1 mmol of HBF₄ were added. The solution was left to stir for one hour and slow diethylether diffusion yielded red needle crystals after 3-4 days (32 mg, 47%). ¹H NMR (400 MHz, CD₃CN): 91.60, 80.19, 38.40, 24.01, 10.51, 8.63, -5.54, -7.64, -16.36, -40,17. Anal. Calcd. for C₈₈H₇₂B₈F₃₂Fe₄N₃₂: C: 42.31; H: 2.91; N, 17.95. Found: C, 44.52; H, 2.74; N, 18.06. MS (+): *m/z* = 1794.3513 (calcd for [Fe₄(HL)₁(L)₃]¹⁺: 1794.3492), 897.67795 (calcd for [Fe₄(HL)₂(L)₂]²⁺: 897.67825), 598.78815 (calcd for [Fe₄(HL)₃(L)₁]³⁺: 598.78793), 449.34257 (calcd for [Fe₄(HL)₄]⁴⁺: 449.34276), 359.67552 (calcd for [Fe₄(HL)₃(H₂L)₁]⁵⁺: 359.67567).

[Fe₄(H₂L)₂(HL)₂](BF₄)₆·8MeCN (Fe-6H). 39.5 mg (0.1 mmol) of ligand H₂L and 37.1 mg (0.11 mmol) of Fe(BF₄)₂·6H₂O were dissolved in 6 mL MeCN under argon. After stirring for 15 minutes, 0.025 mmol of NEt₃ were added. The solution was left to stir for one hour and slow diethylether diffusion yielded red block crystals after 3-4 days (28 mg, 43%). Anal. Calcd. for C₈₈H₇₀B₆F₂₄Fe₄N₃₂: C, 45.52; H, 3.04; N, 19.31. Found: C, 44.96; H, 2.88; N, 19.83.

[Fe₄(HL)₄](BF₄)₄·12MeCN (Fe-4H). 39.5 mg (0.1 mmol) of ligand H₂L and 37.1 mg (0.11 mmol) of Fe(BF₄)₂·6H₂O were dissolved in 6 mL MeCN under argon. After stirring for 15 minutes, 0.05 mmol of NEt₃ were added. The solution was left to stir for one hour and slow diethylether diffusion yielded red plate crystals after a week (22 mg, 33%). ¹H NMR (400 MHz, CD₃CN): 65.81, 52.03, 33.18, 9.36, 6.64, -1.52, -4.15, -10.10. Anal. Calcd. for C₈₈H₆₈B₄F₁₆Fe₄N₃₂: C, 49.25; H, 3.20; N, 20.90. Found: C, 49.63; H, 3.07; N, 21.10.

[Zn₄(H₂L)₄](BF₄)₈·8MeCN (Zn-8H). 39.5 mg (0.1 mmol) of ligand H₂L and 38.2 mg (0.11 mmol) of Zn(BF₄)₂·6H₂O were dissolved in 6 mL MeCN. The solution was left to stir for 30 minutes and slow diethylether diffusion yielded yellow crystals after a few days (27 mg, 38%). Anal. Calcd. for C₈₈H₆₈B₈F₃₂Zn₄N₃₂O₈: C, 39.47; H, 3.31; N, 16.74. Found: C, 39.25; H, 3.31; N, 16.95. ¹H NMR (400 MHz, CD₃CN): 8.03 (t, 1H), 7.87 (t, 2H), 7.81 (s, 2H), 7.75 (d, 2H), 7.73 (t, 1H), 7.58 (d, 2H), 7.25 (t, 2H), 7.14 (t, 1H), 6.49 (d, 1H), 6.29 (s, 1H), 5.59 (d, 1H). MS (+): *m/z* = 916.1603 (calcd for [Zn₄(HL)₂(L)₂]²⁺: 916.1630), 611.1096 (calcd for [Zn₄(HL)₃(L)₁]³⁺: 611.1109), 458,5841 (calcd for [Zn₄(HL)₄]⁴⁺: 458.5851), 367.0688 (calcd for [Zn₄(HL)₃(H₂L)₁]⁵⁺: 367.0696).

[Zn₄(HL)₄](BF₄)₄·8H₂O (Zn-4H). 39.5 mg (0.1 mmol) of ligand H₂L and 38.2 mg (0.11 mmol) of Zn(BF₄)₂·6H₂O were dissolved in 6 mL MeCN. After stirring for 30 minutes, 0.05 mmol of NEt₃ were added. The solution was left to stir for one hour and slow diethylether diffusion yielded red plate crystals after a few days (16 mg, 22 %). Anal. Calcd. for C₈₈H₉₈B₄F₁₆N₃₂O₁₅Zn₄: C, 43.09; H, 4.03; N, 18.27. Found: C, 43.03; H, 3.98; N, 18.39. ¹H NMR (400 MHz, CD₃CN): 7.87 (m, 3H), 7.56 (m, 3H), 7.45 (s, 2H), 7.26 (d, 2H), 7.04 (t, 2H), 6.86 (m, 2H), 5.62 (s, 1H), 5.23 (d, 1H).

FT-IR spectra have been recorded on **Fe-8H**, **Fe-6H** and **Fe-4H** at room temperature in the ATR mode (Figure S1). The intense band observed at ca. 1628 and 1600 cm⁻¹ is typical of an N-H bending vibration and C=C stretching vibration from an aromatic ring of the ligands. The absorption bands at ca. 1462, 1428, 1406, 1380, 1204 and 1139 cm⁻¹ are also characteristic for ligands, blue shift was observed (1468, 1447, 1428, 1406, 1380, 1290, 1194 and 1150 cm⁻¹) when coordinating to the metal centres for **Fe-8H**, **Fe-6H** and **Fe-4H**. The BF₄⁻ ion exhibits four consecutive characteristic peaks at 1096, 1057, 1020 and 937 cm⁻¹. Peaks around 3270 and 3100 cm⁻¹ can be assigned to the N-H stretching vibration of the ligand, whereas those at higher energy are ascribed to H-bonds between the N-H group and the BF₄⁻ ions.

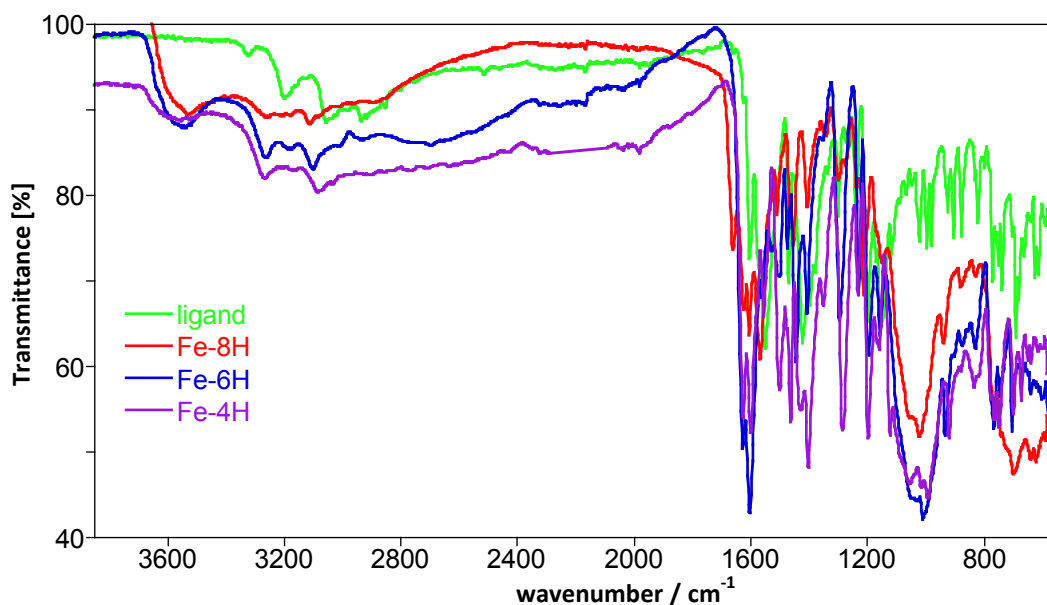


Figure S1. FT-IR spectra of **Fe-8H**, **Fe-6H**, **Fe-4H** and ligand in 3700-550 cm^{-1} ranges.

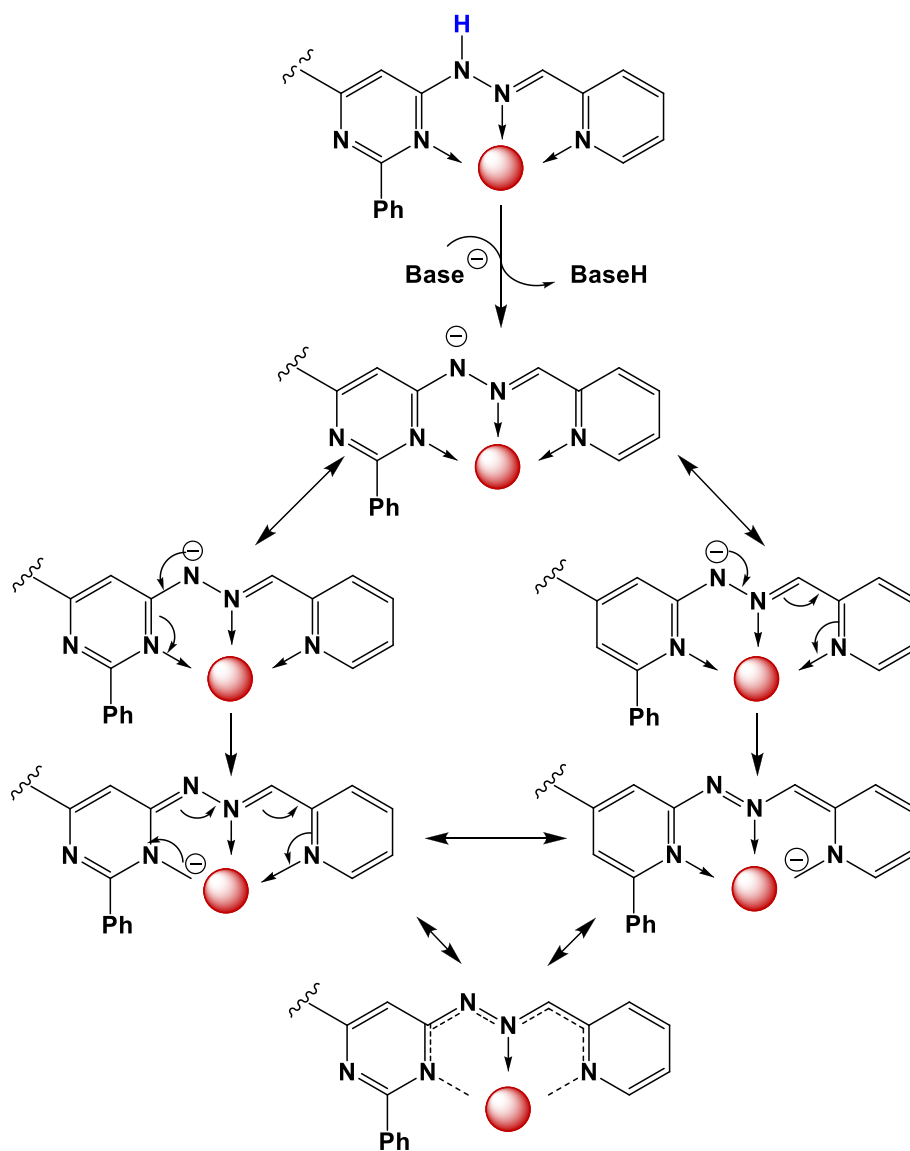
NMR experiments.

Fe-8H titration with DMAN: 1.60 mg of **Fe-8H** was dissolved in a 0.5 mL of a 1:1 mixture of $\text{CD}_3\text{CN}/\text{CDCl}_3$ (1 mM). Aliquots of 5 μL from a 0.05 M solution of Proton Sponge (DMAN) were added (corresponding to 0.5 proton equivalent). **Fe-8H titration with NEt_3 :** 5.44 mg of **Fe-8H** was dissolved in 0.5 mL CD_3CN (4 mM). Aliquots of 10 μL from a 0.2M solution of triethylamine (NEt_3) were added (corresponding to 1 proton equivalent). **Zn-8H titration with NEt_3 :** 1.80 mg of **Zn-8H** was dissolved in either 0.5 mL CD_3CN or 0.5 mL DMSO-d_6 (1.25 mM). Aliquots of 10 μL from a 62.5 mM solution of triethylamine (NEt_3) were added (corresponding to 1 proton equivalent). Magnetic susceptibility was determined by the Evans method^[4] using the equation corrected for a superconducting NMR spectrometer:^[5]

$$\chi_g = -\frac{3\left(\frac{\Delta\nu}{\nu}\right)}{4\pi m} + \chi_s$$

A special double walled NMR tube was used: a sample of pure CD_3CN was placed in the inner tube while the paramagnetic sample solution was placed in the outer tube. The resulting NMR spectrum exhibits two peaks near 2 ppm: one is due to the pure CD_3CN in the inner tube and the other is due to CD_3CN that has been paramagnetically shifted by the paramagnetic sample in the outer tube. The chemical shift of these two peaks was determined

and the separation between them ($\Delta\nu$) measured in hertz (400 MHz NMR: $\nu = 4 \times 10^8$ Hz). The above equation was then used to calculate the gram susceptibility χ_g , which was then converted in to the molar susceptibility (χ). $\chi_0 = -0.534 \times 10^{-6} \text{ cm}^3/\text{g}$ is the gram susceptibility of pure CD_3CN .^[6] The results shown in Figure 4 display error bars obtained from standard deviation over 3 different experiments.



Scheme S1. Deprotonation of an ionizable coordinated terpy-like unit. Red spheres represent Fe or Zn metal ions.

Table S1. Crystallographic data and structural refinement for $[\text{Fe}_4(\text{H}_2\text{L})_4](\text{BF}_4)_8 \cdot 6\text{MeCN}$ (**Fe-8H**; red needles at 120 K), $[\text{Fe}_4(\text{H}_2\text{L})_4](\text{BF}_4)_8 \cdot 2\text{MeCN}$ (**Fe-8H**; red needles at 290 K) and $[\text{Fe}_4(\text{H}_2\text{L})_2(\text{HL})_2](\text{BF}_4)_6 \cdot 8\text{MeCN}$ (**Fe-6H**; red blocks) at 120 and 290 K.

	$[\text{Fe}_4(\text{H}_2\text{L})_4](\text{BF}_4)_8 \cdot 6\text{MeCN}$	$[\text{Fe}_4(\text{H}_2\text{L})_4](\text{BF}_4)_8 \cdot 2\text{MeCN}$	$[\text{Fe}_4(\text{H}_2\text{L})_2(\text{HL})_2](\text{BF}_4)_6 \cdot 8\text{MeCN}$	
	Fe-8H	Fe-8H	Fe-6H	
CCDC Number	1560748	1560744	1560746	1560745
Formula	$\text{C}_{100}\text{H}_{90}\text{B}_8\text{F}_{32}\text{Fe}_4\text{N}_{38}$	$\text{C}_{92}\text{H}_{78}\text{B}_8\text{F}_{32}\text{Fe}_4\text{N}_{34}$	$\text{C}_{104}\text{H}_{94}\text{B}_6\text{F}_{24}\text{Fe}_4\text{N}_{40}$	
MW / g mol⁻¹	2741.97	2577.76	2648.45	
Crystal system	monoclinic	monoclinic	monoclinic	
Space group	<i>C2/c</i>	<i>C2/c</i>	<i>P2₁/c</i>	
Colour, shape	red needle	red needle	red block	
Wavelength / Å	0.71073	0.71073	0.71073	
Crystal size / mm³	0.20 x 0.08 x 0.04	0.20 x 0.08 x 0.04	0.10 x 0.09 x 0.09	
Temperature / K	120(2)	290(2)	120(2)	290(2)
a / Å	20.0311(15)	17.479(3)	26.4577(10)	26.948(2)
b / Å	35.230(3)	36.198(6)	17.6215(7)	17.7359(15)
c / Å	18.0924(14)	18.614(3)	27.3241(11)	27.532(2)
β / °	111.188(4)	108.768(6)	116.132(2)	115.376(4)
v / Å³	11904.6(17)	11151(3)	11437.0(8)	11889.2(18)
d_{calc} / g cm⁻³	1.530	1.535	1.538	1.480
Z	4	4	4	4
Unique reflections	6383	5982	23464	24571
Parameters; Restraints	794; 41	790; 48	1676;132	1623; 28
R₁^a [all data]	0.1052	0.1241	0.1079	0.1363
wR₂^b [all data]	0.2538	0.2350	0.2165	0.1915
R₁^a [I > 2σ(I)]	0.0926	0.0750	0.0758	0.0703
wR₂^b [I > 2σ(I)]	0.2441	0.1916	0.1922	0.1622
GOF on F²	1.078	1.106	1.013	1.023
^a $R_1 = \sum F_o - F_c / \sum F_o $. ^b $wR_2 = (\sum [w(F_o^2 - F_c^2)^2] / \sum [w(F_o^2)^2])^{1/2}$				

Table S2. Crystallographic data and structural refinement for **[Fe₄(HL)₄](BF₄)₄·12MeCN (Fe-4H; red plates).**

	[Fe₄(HL)₄](BF₄)₄·12MeCN Fe-4H
CCDC Number	1560747
Formula	C ₁₁₂ H ₁₀₄ B ₄ F ₁₆ Fe ₄ N ₄₄
MW / g mol⁻¹	2637.03
Crystal system	monoclinic
Space group	<i>P</i> 2 ₁ / <i>c</i>
Colour, shape	red plate
Wavelength / Å	0.71073
Temperature / K	120(2)
<i>a</i> / Å	17.5399(8)
<i>b</i> / Å	25.9317(11)
<i>c</i> / Å	28.7826(12)
<i>α</i> / °	90
<i>β</i> / °	116.955(3)
<i>γ</i> / °	90
<i>V</i> / Å³	11669.2(9)
<i>d</i>_{calc} / g cm⁻³	1.501
<i>Z</i>	4
Unique reflections	16860
Parameters; Restraints	1502; 349
<i>R</i>₁^a [all data]	0.1271
<i>wR</i>₂^b [all data]	0.2586
<i>R</i>₁^a [<i>I</i> > 2σ(<i>I</i>)]	0.0921
<i>wR</i>₂^b [<i>I</i> > 2σ(<i>I</i>)]	0.2415
GOF on <i>F</i>²	1.064

Table S3. Selected interatomic distances (Å) for **Fe-8H** in $[\text{Fe}_4(\text{H}_2\text{L})_4](\text{BF}_4)_8 \cdot 6\text{MeCN}$ (at 120 K) and $[\text{Fe}_4(\text{H}_2\text{L})_4](\text{BF}_4)_8 \cdot 2\text{MeCN}$ (at 290 K)

	$[\text{Fe}_4(\text{H}_2\text{L})_4](\text{BF}_4)_8 \cdot 6\text{MeCN}$	$[\text{Fe}_4(\text{H}_2\text{L})_4](\text{BF}_4)_8 \cdot 2\text{MeCN}$
Fe1-N2	1.885(9)	2.099(9)
Fe1-N7	1.888(8)	2.081(8)
Fe1-N1	1.985(7)	2.178(9)
Fe1-N6	2.004(10)	2.165(8)
Fe1-N4	2.055(7)	2.196(8)
Fe1-N9	2.060(7)	2.184(7)
Fe2-N12	1.971(7)	1.999(8)
Fe2-N15	1.972(8)	1.980(8)
Fe2-N13	2.023(9)	2.069(9)
Fe2-N14	2.041(7)	2.085(8)
Fe2-N5	2.104(8)	2.116(8)
Fe2-N10	2.133(7)	2.127(8)

Table S4. Selected interatomic distances (Å) for **Fe-6H** at 120 and 290 K.

	120 K	290 K
Fe1-N31	1.875(3)	1.872(4)
Fe1-N2	1.878(3)	1.871(4)
Fe1-N1	1.958(4)	1.963(4)
Fe1-N32	1.986(3)	1.994(4)
Fe1-N29	2.031(3)	2.026(4)
Fe1-N4	2.035(3)	2.043(4)
Fe2-N7	2.010(4)	2.118(4)
Fe2-N11	2.021(6)	2.122(4)
Fe2-N8	2.093(4)	2.201(4)
Fe2-N9	2.109(5)	2.240(4)
Fe2-N12	2.120(5)	2.187(4)
Fe2-N5	2.165(4)	2.247(4)
Fe3-N18	1.872(4)	1.871(4)
Fe3-N15	1.886(4)	1.885(4)
Fe3-N17	1.977(4)	1.971(4)
Fe3-N16	1.979(4)	1.984(4)
Fe3-N13	2.036(4)	2.026(4)
Fe3-N20	2.063(4)	2.053(4)
Fe4-N26	1.904(6)	2.088(4)
Fe4-N23	1.907(6)	2.088(4)
Fe4-N24	1.986(5)	2.197(4)
Fe4-N25	2.029(5)	2.204(4)
Fe4-N28	2.078(4)	2.191(4)
Fe4-N21	2.113(4)	2.244(4)

Table S5. Selected interatomic distances (Å) for **Fe-4H** at 120 K.

	120 K
Fe1-N31	1.876(7)
Fe1-N2	1.840(7)
Fe1-N1	1.955(6)
Fe1-N32	1.994(6)
Fe1-N29	2.036(5)
Fe1-N4	2.022(5)
Fe2-N7	2.068(6)
Fe2-N10	2.081(7)
Fe2-N8	2.162(6)
Fe2-N9	2.172(6)
Fe2-N12	2.190(6)
Fe2-N5	2.172(6)
Fe3a-N18a	1.912(14)
Fe3a-N15a	1.882(13)
Fe3a-N17a	1.963(13)
Fe3a-N16a	2.012(14)
Fe3a-N13	1.924(12)
Fe3a-N20	2.206(10)
Fe3b-N18 b	1.910(14)
Fe3b-N15b	1.875(13)
Fe3b-N17b	1.949(13)
Fe3b-N16b	2.017(14)
Fe3b-N13	2.126(12)
Fe3b-N20	1.880(11)
Fe4-N26	2.086(6)
Fe4-N23	2.093(7)
Fe4-N24	2.179(6)
Fe4-N25	2.184(6)
Fe4-N28	2.197(6)
Fe4-N21	2.176(6)

Table S6. Crystallographic data and structural refinement for $[\text{Zn}_4(\text{H}_2\text{L})_4](\text{BF}_4)_8 \cdot 8\text{MeCN}$ (**Zn-8H**; orange prisms) at 173 K and $[\text{Zn}_4(\text{HL})_4](\text{BF}_4)_4 \cdot 8\text{H}_2\text{O}$ (**Zn-4H**; red blocks) at 120 K.

	$[\text{Zn}_4(\text{H}_2\text{L})_4](\text{BF}_4)_8 \cdot 8\text{MeCN}$ Zn-8H	$[\text{Zn}_4(\text{HL})_4](\text{BF}_4)_4 \cdot 8\text{H}_2\text{O}$ Zn-4H
CCDC Number	1835254	1835255
Formula	$\text{C}_{104}\text{H}_{96}\text{B}_8\text{F}_{32}\text{Zn}_4\text{N}_{40}$	$\text{C}_{88}\text{H}_{84}\text{B}_4\text{F}_{16}\text{N}_{32}\text{O}_8\text{Zn}_4$
MW / g mol⁻¹	2862.15	2326.59
Crystal system	monoclinic	tetragonal
Space group	$P2_1/c$	$P4_n/cc$
Colour, shape	orange prism	red block
Wavelength / Å	1.54178	0.71073
Crystal size / mm³	0.36 x 0.20 x 0.12	0.30 x 0.14 x 0.10
Temperature / K	173(2)	120(2)
<i>a</i> / Å	19.5838(5)	21.6393(13)
<i>b</i> / Å	35.6460(10)	21.6393(13)
<i>c</i> / Å	18.5501(5)	21.1688(15)
α / °	90	90
β / °	110.798(2)	90
γ / °	90	90
<i>V</i> / Å³	12105.7(6)	9912.5(14)
<i>d</i>_{calc} / g cm⁻³	1.458	1.511
<i>Z</i>	4	4
Unique reflections	21271	4911
Parameters; Restraints	1429; 11	340; 3
<i>R</i>₁^a [all data]	0.1458	0.0623
<i>wR</i>₂^b [all data]	0.2674	0.1589
<i>R</i>₁^a [<i>I</i> > 2σ(<i>I</i>)]	0.1211	0.0604
<i>wR</i>₂^b [<i>I</i> > 2σ(<i>I</i>)]	0.2573	0.1574
GOF on <i>F</i>²	1.045	1.138

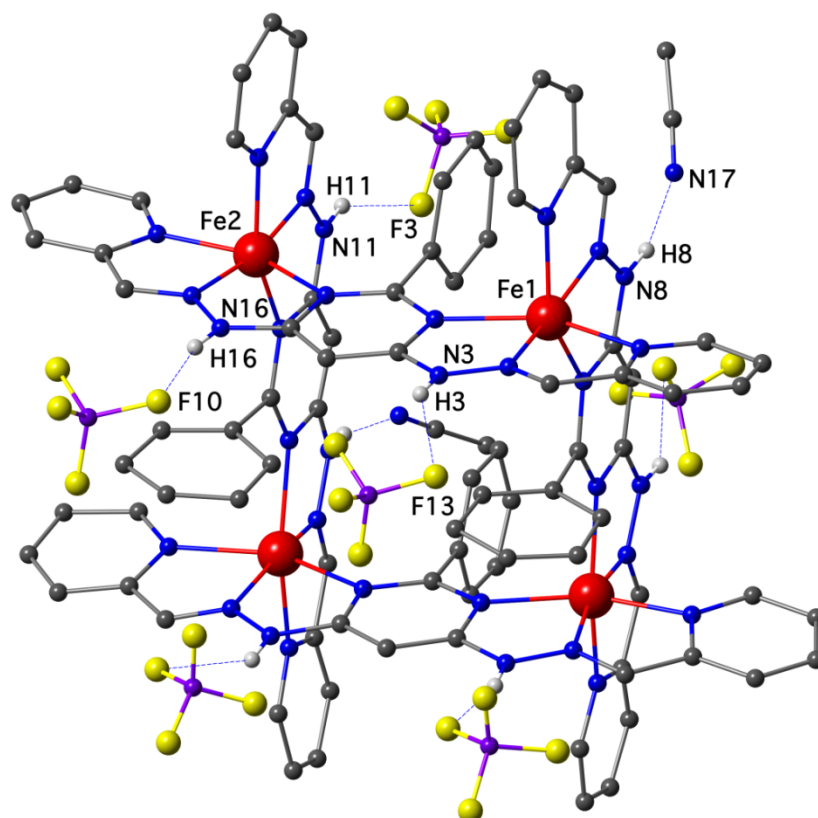


Figure S2. Ball and stick representation of the crystal structure of $[\text{Fe}_4(\text{H}_2\text{L})_4](\text{BF}_4)_8 \cdot 2\text{MeCN}$ complex (**Fe-8H**; at 290 K) evidencing the hydrogen bonding between NH sites and acetonitrile and tetrafluoroborate molecules. Fe, N, C, B, F and H atoms are shown in red, blue, grey, purple, yellow and white, respectively. All non-NH hydrogen atoms and non-interacting lattice molecules are omitted for clarity. Corresponding distances: $\text{N8} \cdots \text{N17} = 2.89 \text{ \AA}$, $\text{N3} \cdots \text{F13} = 3.00 \text{ \AA}$, $\text{N11} \cdots \text{F3} = 3.04 \text{ \AA}$, $\text{N16} \cdots \text{F10} = 2.81 \text{ \AA}$. Corresponding angles: $\text{N8-H8} \cdots \text{N17} = 164.6^\circ$, $\text{N3-H3} \cdots \text{F13} = 144.3^\circ$, $\text{N11-H11} \cdots \text{F3} = 146.7^\circ$, $\text{N16-H16} \cdots \text{F10} = 166.2^\circ$.

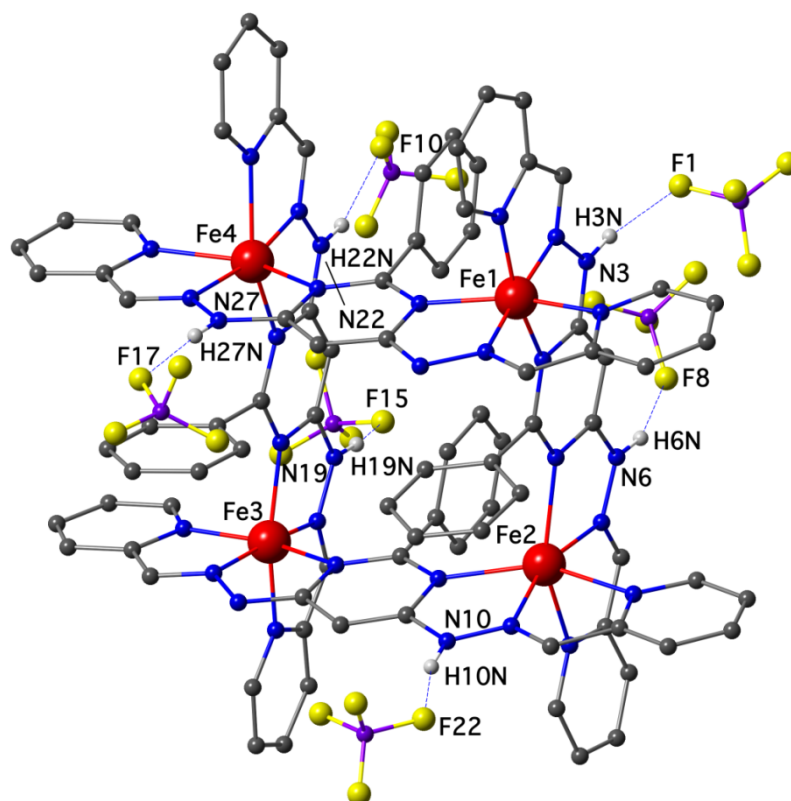


Figure S3. Ball and stick representation of the crystal structure of $[\text{Fe}_4(\text{H}_2\text{L})_2(\text{HL})_2](\text{BF}_4)_6 \cdot 8\text{MeCN}$ complex (**Fe-6H**; at 290 K) evidencing the hydrogen bonding between NH sites and tetrafluoroborate molecules. Fe, N, C, B, F and H atoms are shown in red, blue, grey, purple, light green and white, respectively. All non-NH hydrogen atoms and non-interacting lattice molecules are omitted for clarity. Corresponding distances: $\text{N3} \cdots \text{F1} = 2.71 \text{ \AA}$, $\text{N6} \cdots \text{F8} = 2.77 \text{ \AA}$, $\text{N10} \cdots \text{F22} = 2.80 \text{ \AA}$, $\text{N19} \cdots \text{F15} = 2.71 \text{ \AA}$, $\text{N22} \cdots \text{F10} = 2.85 \text{ \AA}$, $\text{N27} \cdots \text{F17} = 2.75 \text{ \AA}$. Corresponding angles: $\text{N3-H3N} \cdots \text{F1} = 158.5^\circ$, $\text{N6-H6N} \cdots \text{F8} = 160.4^\circ$, $\text{N10-H10N} \cdots \text{F22} = 161.9^\circ$, $\text{N19-H19N} \cdots \text{F15} = 165.6^\circ$, $\text{N22-H22N} \cdots \text{F10} = 154.8^\circ$, $\text{N27-H27N} \cdots \text{F17} = 171.2^\circ$.

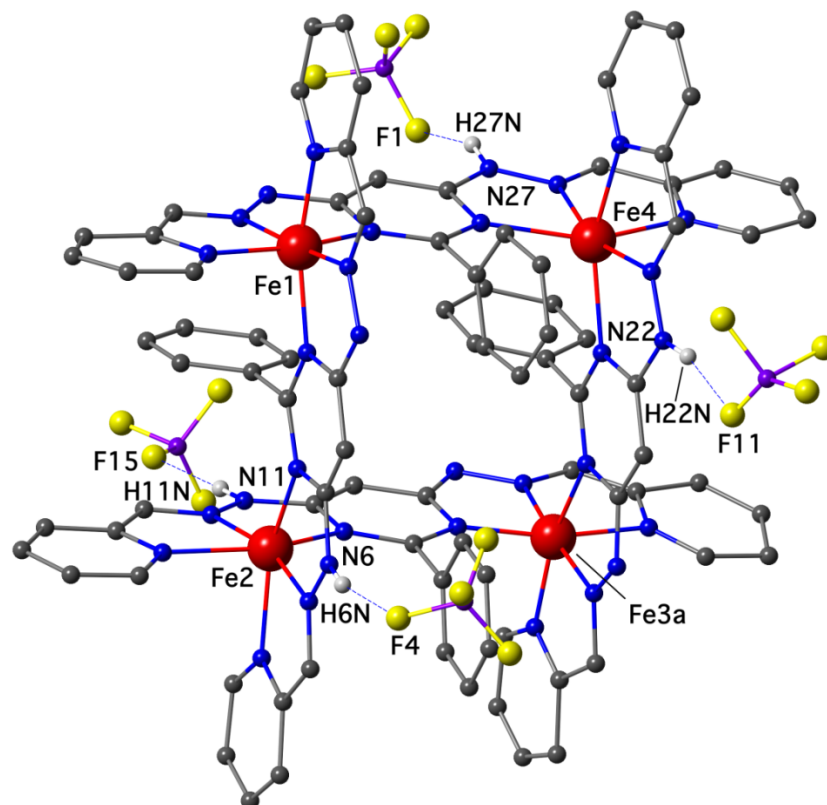


Figure S4. Ball and stick representation of the crystal structure of $[\text{Fe}_4(\text{HL})_4](\text{BF}_4)_4 \cdot 12\text{MeCN}$ complex (**Fe-4H**; at 120 K) evidencing the hydrogen bonding between NH sites and tetrafluoroborate molecules. Fe, N, C, B, F and H atoms are shown in red, blue, grey, purple, light green and white, respectively. All non-NH hydrogen atoms and non-interacting lattice molecules are omitted for clarity. Corresponding distances: $\text{N11} \cdots \text{F15} = 2.89 \text{ \AA}$, $\text{N6} \cdots \text{F4} = 2.79 \text{ \AA}$, $\text{N22} \cdots \text{F11} = 2.80 \text{ \AA}$, $\text{N27} \cdots \text{F1} = 2.81 \text{ \AA}$. Corresponding angles: $\text{N11-H11N} \cdots \text{F15} = 171.0^\circ$, $\text{N6-H6N} \cdots \text{F4} = 163.5^\circ$, $\text{N22-H22N} \cdots \text{F11} = 164.7^\circ$, $\text{N27-H27N} \cdots \text{F1} = 155.7^\circ$.

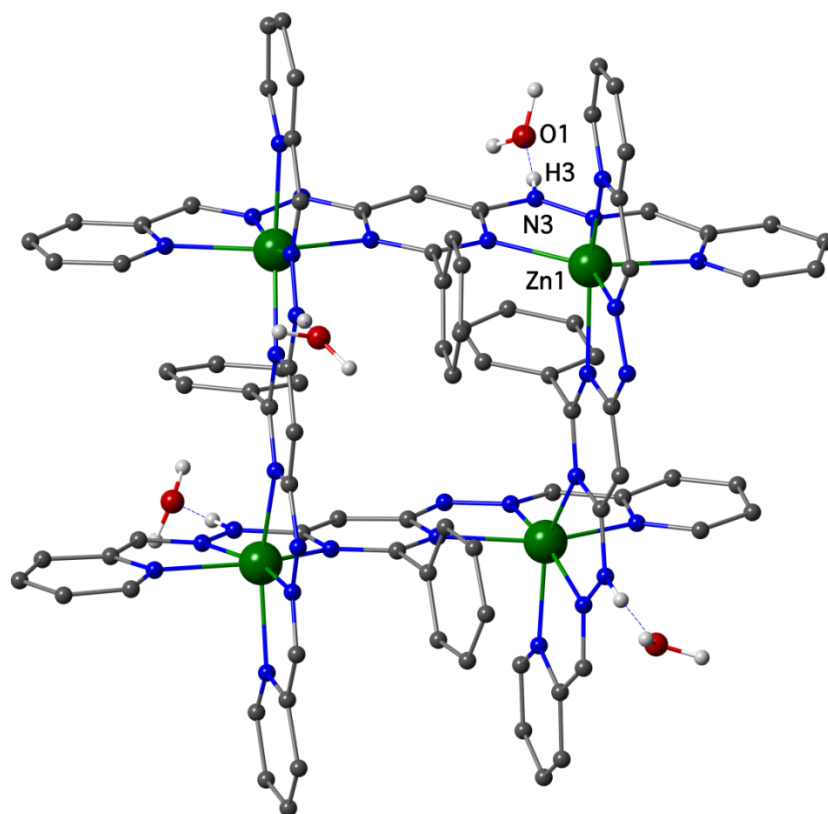


Figure S5. Ball and stick representation of the crystal structure of $[\text{Zn}_4(\text{HL})_4](\text{BF}_4)_4 \cdot 8\text{H}_2\text{O}$ complex (**Zn-4H**; at 120 K) evidencing the hydrogen bonding between NH sites and water molecules. Zn, N, C, O and H atoms are shown in green, blue, grey, dark red and white, respectively. All non-NH hydrogen atoms and non-interacting lattice molecules are omitted for clarity. Corresponding distance: $\text{N3} \cdots \text{O1} = 2.71 \text{ \AA}$. Corresponding angle: $\text{N3-H3} \cdots \text{O1} = 176.1^\circ$.

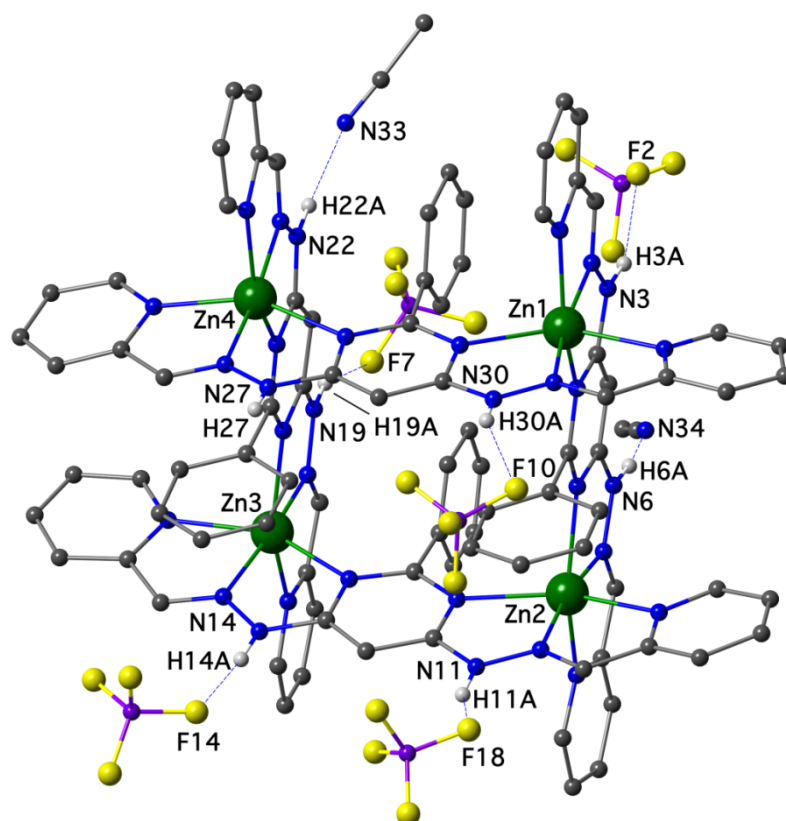


Figure S6. Ball and stick representation of the crystal structure of $[\text{Zn}_4(\text{H}_2\text{L})_4](\text{BF}_4)_8 \cdot 8\text{MeCN}$ complex (**Zn-8H**; at 173 K) evidencing the hydrogen bonding between NH sites and tetrafluoroborate and acetonitrile molecules. Zn, N, C, B, F and H atoms are shown in green, blue, grey, purple, light green and white, respectively. All non-NH hydrogen atoms and non-interacting lattice molecules are omitted for clarity. Corresponding distances: $\text{N3} \cdots \text{F2} = 2.88 \text{ \AA}$, $\text{N30} \cdots \text{F10} = 3.00 \text{ \AA}$, $\text{N6} \cdots \text{N34} = 2.89 \text{ \AA}$, $\text{N11} \cdots \text{F18} = 2.85 \text{ \AA}$, $\text{N14} \cdots \text{F14} = 2.78 \text{ \AA}$, $\text{N19} \cdots \text{F7} = 2.87 \text{ \AA}$, $\text{N22} \cdots \text{N33} = 2.93 \text{ \AA}$. Corresponding angles: $\text{N3-H3A} \cdots \text{F2} = 151.7^\circ$, $\text{N30-H30A} \cdots \text{F10} = 152.5^\circ$, $\text{N6-H6A} \cdots \text{N34} = 165.9^\circ$, $\text{N11-H11A} \cdots \text{F18} = 148.7^\circ$, $\text{N14-H14A} \cdots \text{F14} = 173.5^\circ$, $\text{N19-H19A} \cdots \text{F7} = 153.4^\circ$, $\text{N22-H22A} \cdots \text{N33} = 166.6^\circ$.

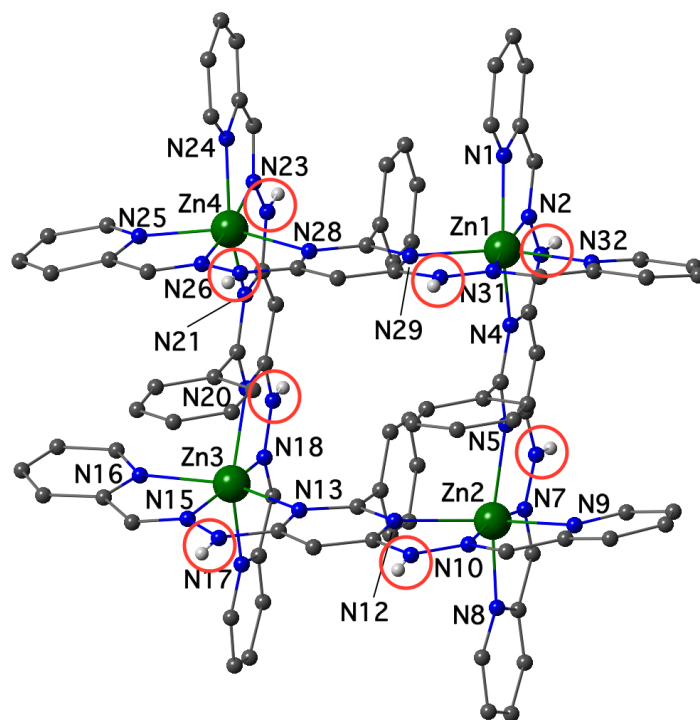


Figure S7. Ball and stick representation of the crystal structure of $[\text{Zn}_4(\text{H}_2\text{L})_4](\text{BF}_4)_8 \cdot 8\text{MeCN}$ (**Zn-8H**; at 173 K). Zn, N, C and H atoms are shown in green, blue, grey and white, respectively. Acetonitrile molecules and tetrafluoroborate anions are omitted for clarity.

Table S7. Shape $S(O_h)$ Parameters for all crystal structures (it is worth noting that values of $S(O_h)$ smaller than 4.42 indicate a geometry closer to the octahedron than to the trigonal prism and thus these systems are best described as a distorted octahedron. Conversely, geometry with $S(O_h) > 4.42$ should be termed distorted trigonal prisms).^[7]

	Fe-8H 120 K	Fe-6H 120 K	Fe-4H 120 K	Fe-6H 290 K	Fe-8H 290 K	Zn-8H 173 K	Zn-4H 120 K
M1	2.66	2.24	2.46	2.41	5.79	6.07	5.27
M2	3.72	4.55	5.45	6.19	3.88	5.58	-
M3	-	2.44	5.68 ^a	2.40	-	5.76	-
M4	-	2.78	2.32	5.52	-	8.81	-
Avg.	3.19	3.00	3.98	4.13	4.84	6.07	5.27

Notes: M being Fe or Zn. The Fe3 and Fe4 sites are symmetry equivalent to Fe1 and Fe2 sites in **Fe-8H**. The Zn2, Zn3 and Zn4 sites are symmetry equivalent to the Zn1 site in **Zn-4H**. ^a The structure of **Fe-4H** at 120K contains two disordered Fe3 site. The quoted value corresponds to the Fe3A site.

Additional magnetic measurements

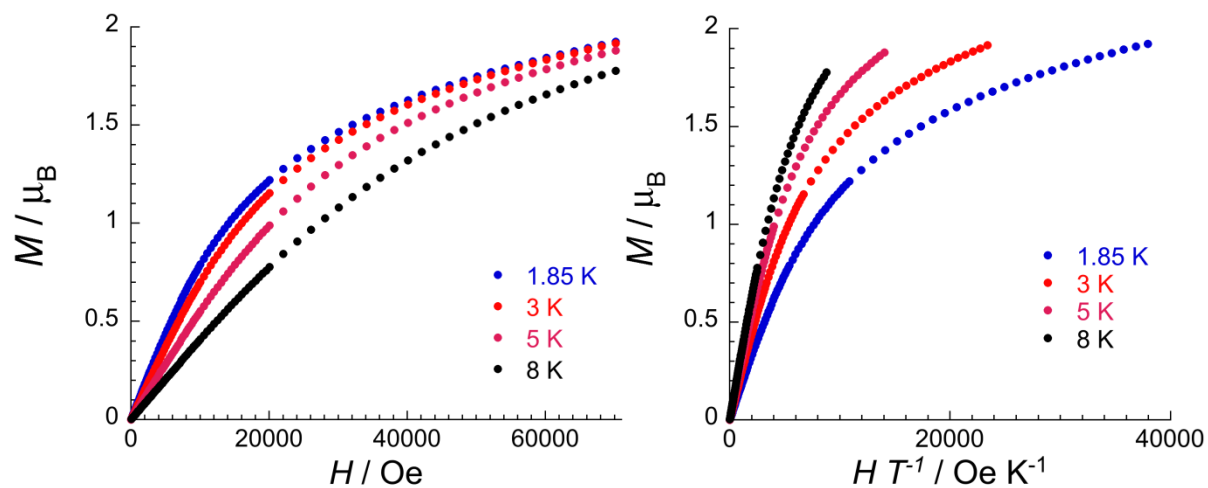


Figure S8. Field dependence of magnetization for **Fe-8H** plotted as M versus H (left) or M versus H/T (right) at the temperatures indicated, scanning at $80 - 400 \text{ Oe}\cdot\text{min}^{-1}$ for $H < 1 \text{ T}$ and $500 - 2500 \text{ Oe}\cdot\text{min}^{-1}$ for $H > 1 \text{ T}$.

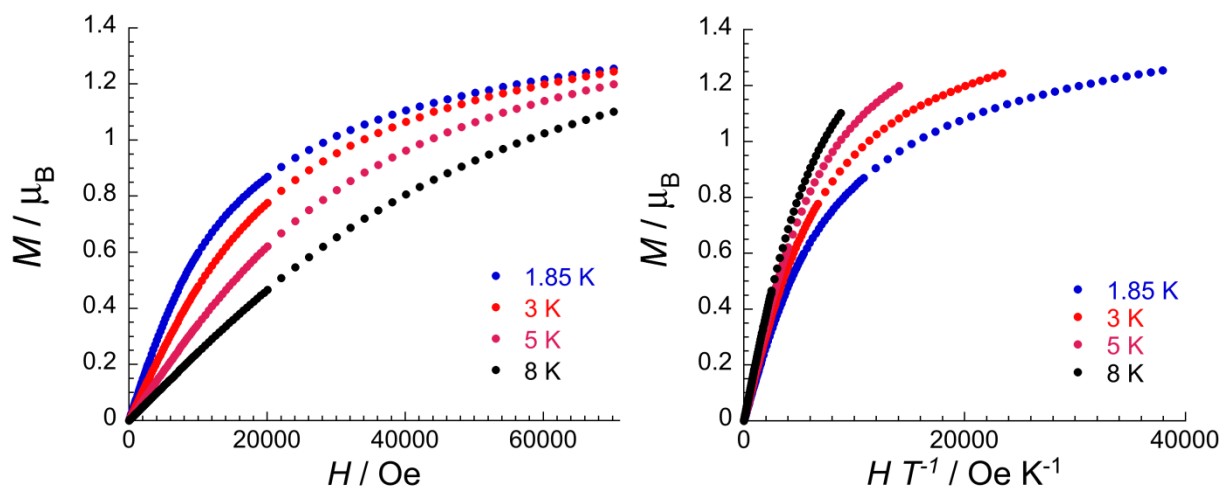


Figure S9. Field dependence of magnetization for **Fe-6H** plotted as M versus H (left) or M versus H/T (right) at the temperatures indicated, scanning at $80 - 400 \text{ Oe}\cdot\text{min}^{-1}$ for $H < 1 \text{ T}$ and $500 - 2500 \text{ Oe}\cdot\text{min}^{-1}$ for $H > 1 \text{ T}$.

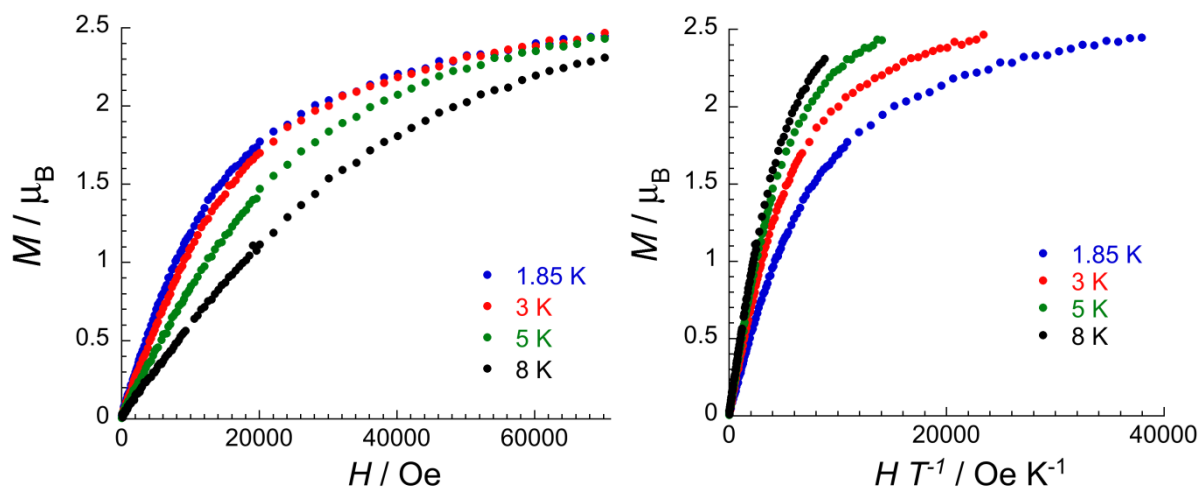


Figure S10. Field dependence of magnetization for **Fe-4H** plotted as M versus H (left) or M versus H/T (right) at the temperatures indicated, scanning at $80 - 400 \text{ Oe}\cdot\text{min}^{-1}$ for $H < 1 \text{ T}$ and $500 - 2500 \text{ Oe}\cdot\text{min}^{-1}$ for $H > 1 \text{ T}$.

UV-Vis spectra of the grid $[\text{Fe}_4(\text{H}_2\text{L})_4]^{8+}$ (Figure S7) have been measured between $\text{pH} = 1$ and $\text{pH} = 13$ in a 50 :50 (v/v) mixture of acetonitrile and Britton-Robinson buffer.^[8] From $\text{pH} = 8$ onwards no change in the spectrum can be observed, which means that the grid is fully deprotonated. The grid $[\text{Fe}_4(\text{H}_2\text{L})_4]^{8+}$ exhibits an absorption band at 387 nm, which can be attributed to the fully protonated grid complex. Another band appears at 455 nm, which first augments in intensity until $\text{pH} = 4$, and after diminishes when going towards more basic pH. Around the same value of $\text{pH} = 4$, a third band at 521 nm starts increasing in intensity until reaching a maximum intensity at $\text{pH} = 8$. Considering the ratio of molar absorption coefficient and the λ_{max} obtained, and comparing it to the values known for $[\text{Fe}(\text{Hpaphy})_2]^{2+}$ et $[\text{Fe}(\text{paphy})_2]$ (Table S8), these charge transfer bands observed appear to be MLCT type (Metal Ligand Charge Transfer).

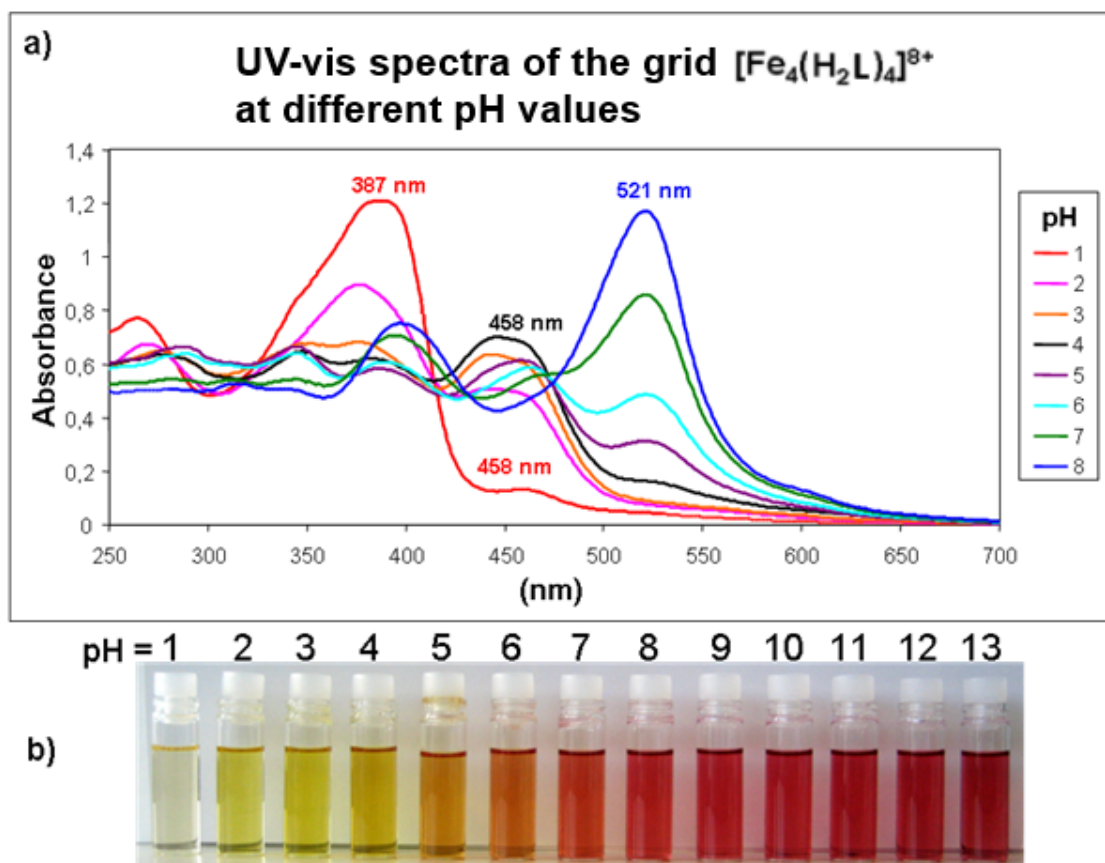


Figure S11. (a) UV-Vis spectra of the grid $[\text{Fe}_4(\text{H}_2\text{L})_4]^{8+}$ at $1 < \text{pH} < 8$ in a 50:50 (v/v) mixture of acetonitrile and Britton-Robinson buffer; (b) pictures of solution at $1 < \text{pH} < 13$.

Table S8. λ_{max} et ϵ values for grid $[\text{Fe}_4(\text{H}_2\text{L})_4]^{8+}$ and $[\text{Fe}(\text{Hpaphy})_2]^{2+}$.

Base eq.	$\epsilon / \text{M}^{-1} \text{cm}^{-1}$ $[\text{Fe}_4(\text{H}_2\text{L})_4]^{8+}$	
	$\lambda = 458 \text{ nm}$	$\lambda = 521 \text{ nm}$
0	69 173	-----
8	-----	114 489

$\epsilon / \text{M}^{-1} \text{cm}^{-1}$ $[\text{Fe}(\text{Hpaphy})_2]^{2+}$	$\epsilon / \text{M}^{-1} \text{cm}^{-1}$ $[\text{Fe}(\text{paphy})_2]$
$\lambda = 524 \text{ nm}$	$\lambda = 603 \text{ nm}$
6 900	4050

Mass spectrometry

The mass spectrum of **Fe-8H** is detailed below. The fully protonated grid is **Fe-8H** exhibiting an 8+ charge due to four Fe^{II} metal ions ($[\text{Fe}_4(\text{H}_2\text{L})_4]^{8+}$). The deprotonation of the grid still gives a positive cation with a decreasing charge following an increasing deprotonation. Five different cations are observed, corresponding to the grid deprotonated 3 to 7 times, as shown in the table below:

Grid cation	Chemical Formula	m/z
$[\text{Fe}_4(\text{HL})_3(\text{H}_2\text{L})_1]^{5+}$	$\text{C}_{88}\text{H}_{69}\text{N}_{32}\text{Fe}_4$	1794.3513
$[\text{Fe}_4(\text{HL})_4]^{4+}$	$\text{C}_{88}\text{H}_{68}\text{N}_{32}\text{Fe}_4$	897.6779
$[\text{Fe}_4(\text{HL})_3(\text{L})_1]^{3+}$	$\text{C}_{88}\text{H}_{69}\text{N}_{32}\text{Fe}_4$	598.7880
$[\text{Fe}_4(\text{HL})_2(\text{L})_2]^{2+}$	$\text{C}_{88}\text{H}_{69}\text{N}_{32}\text{Fe}_4$	449.3425
$[\text{Fe}_4(\text{HL})_1(\text{L})_3]^{1+}$	$\text{C}_{88}\text{H}_{69}\text{N}_{32}\text{Fe}_4$	355.0973

Mass spectra for **Fe-8H**, **Fe-6H** and **Fe-4H** gave similar results (in the case of **Fe-4H** it was not possible to identify the peaks corresponding to $[\text{Fe}_4(\text{HL})_1(\text{L})_3]^{1+}$, as the grid species get deprotonated during the analysis. The same cations were obtained with **Zn-8H** (**Zn-4H** is also identical to **Zn-8H**, similarly to the results obtained for the **Fe-nH** analogues). MS (+): $m/z = 916.1603$ (calcd for $[\text{Zn}_4(\text{HL})_2(\text{L})_2]^{2+}$: 916.1630), 611.1096 (calcd for $[\text{Zn}_4(\text{HL})_3(\text{L})_1]^{3+}$: 611.1109), 458.5841 (calcd for $[\text{Zn}_4(\text{HL})_4]^{4+}$: 458.5851), 367.0688 (calcd for $[\text{Zn}_4(\text{HL})_3(\text{H}_2\text{L})_1]^{5+}$: 367.0696).

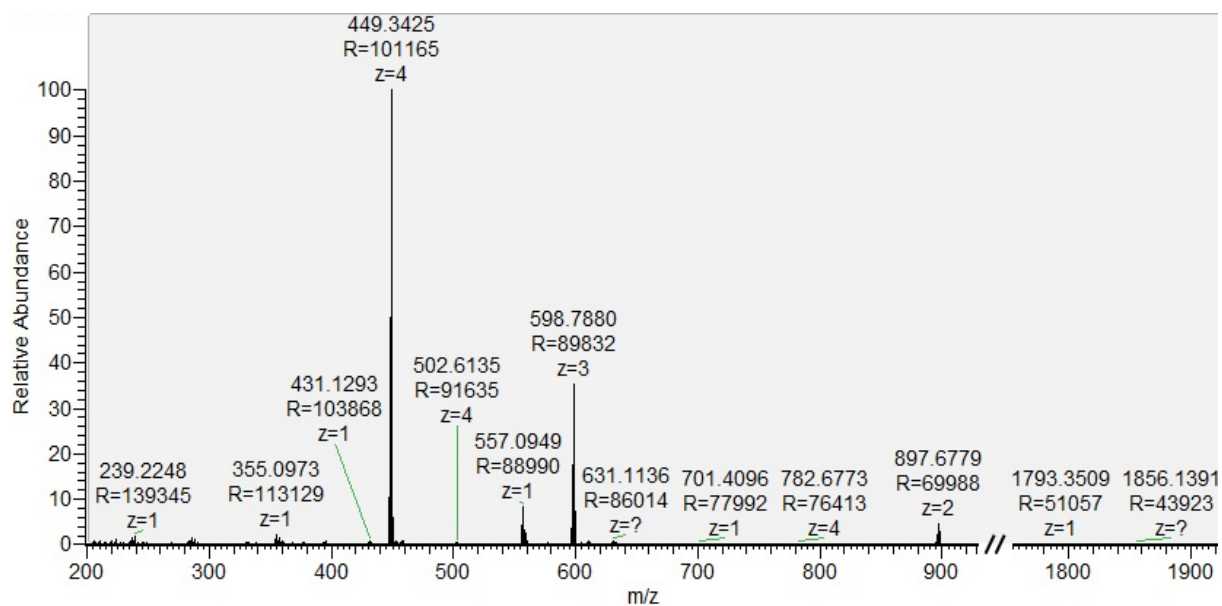


Figure S12. Mass spectrum of **Fe-8H** and detailed fit for all five cations $[\text{Fe}_4(\text{HL})_3(\text{H}_2\text{L})_1]^{5+}$, $[\text{Fe}_4(\text{HL})_4]^{4+}$, $[\text{Fe}_4(\text{HL})_3(\text{L})_1]^{3+}$, $[\text{Fe}_4(\text{HL})_2(\text{L})_2]^{2+}$ and $[\text{Fe}_4(\text{HL})_1(\text{L})_3]^{1+}$.

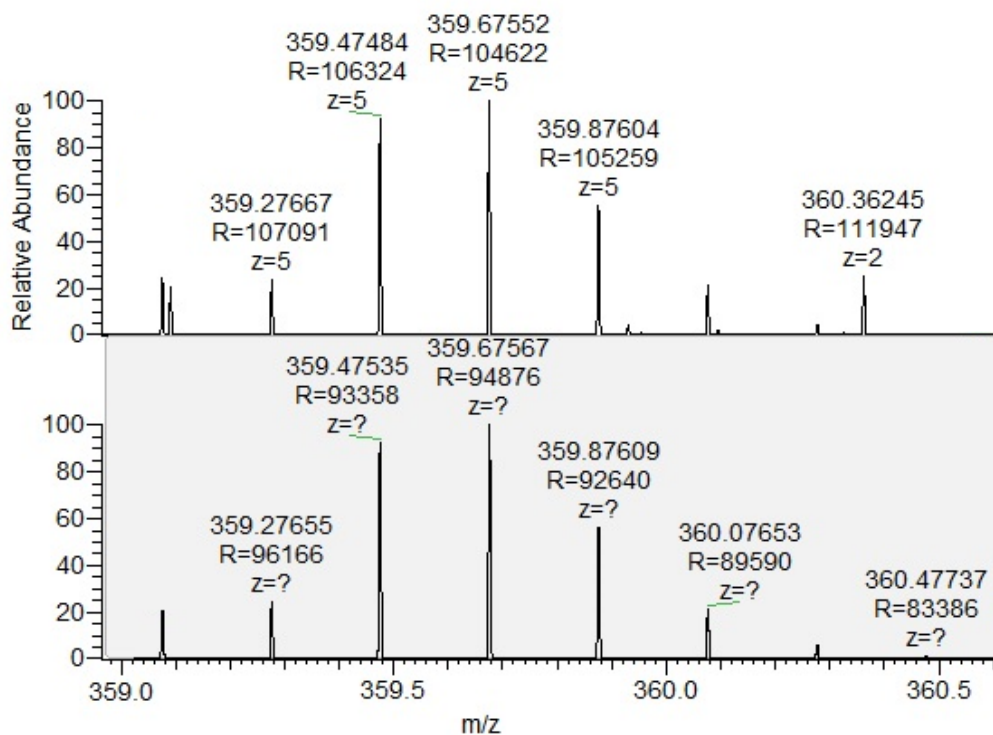


Figure S13. Mass spectrum of **Fe-8H** (top) and calculated isotope pattern for $[\text{Fe}_4(\text{HL})_3(\text{H}_2\text{L})_1]^{5+}$ (bottom).

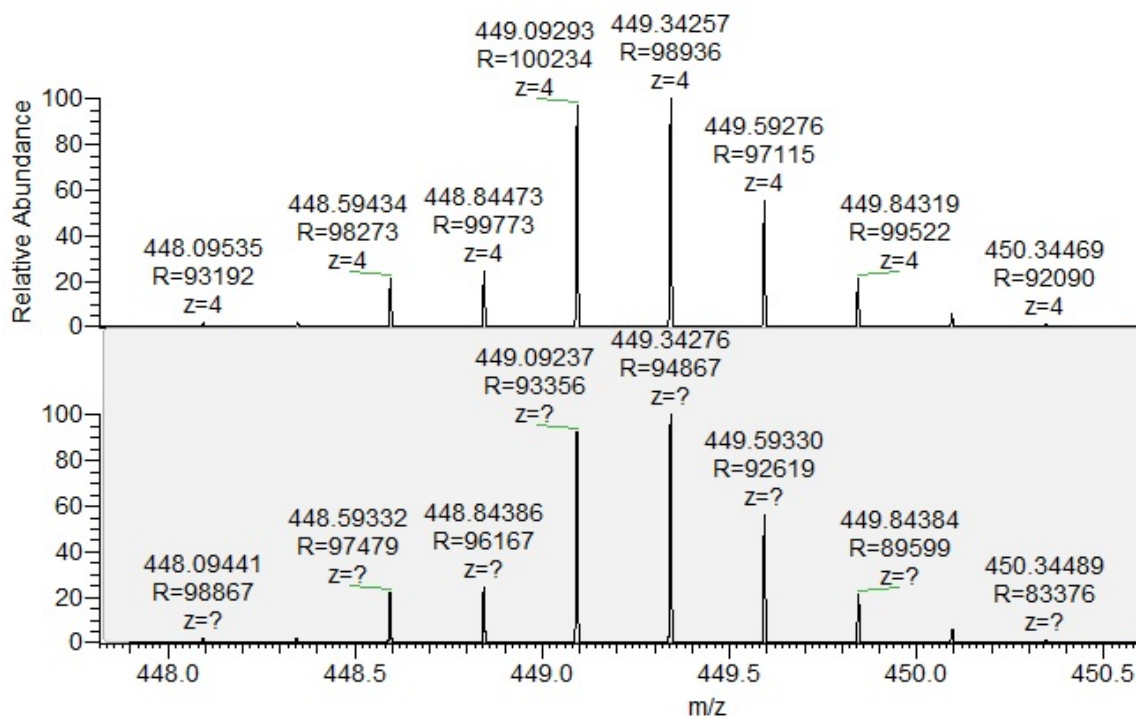


Figure S14. Mass spectrum of **Fe-8H** (top) and calculated isotope pattern for $[\text{Fe}_4(\text{HL})_4]^{4+}$ (bottom).

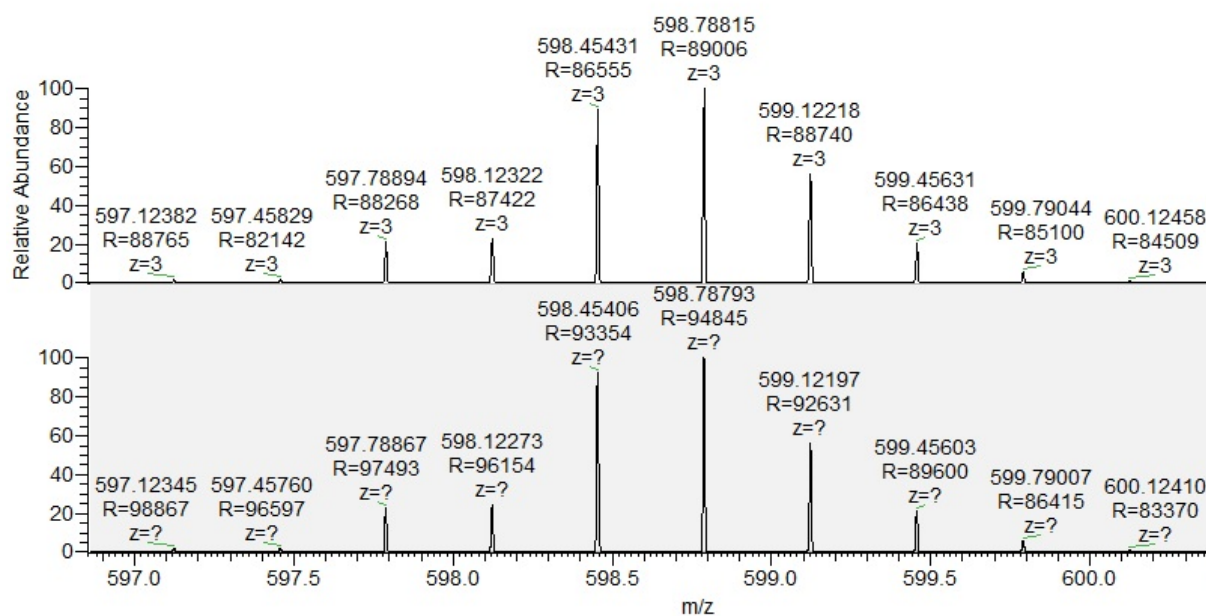


Figure S15. Mass spectrum of **Fe-8H** (top) and calculated isotope pattern for $[\text{Fe}_4(\text{HL})_3(\text{L})]^{3+}$ (bottom).

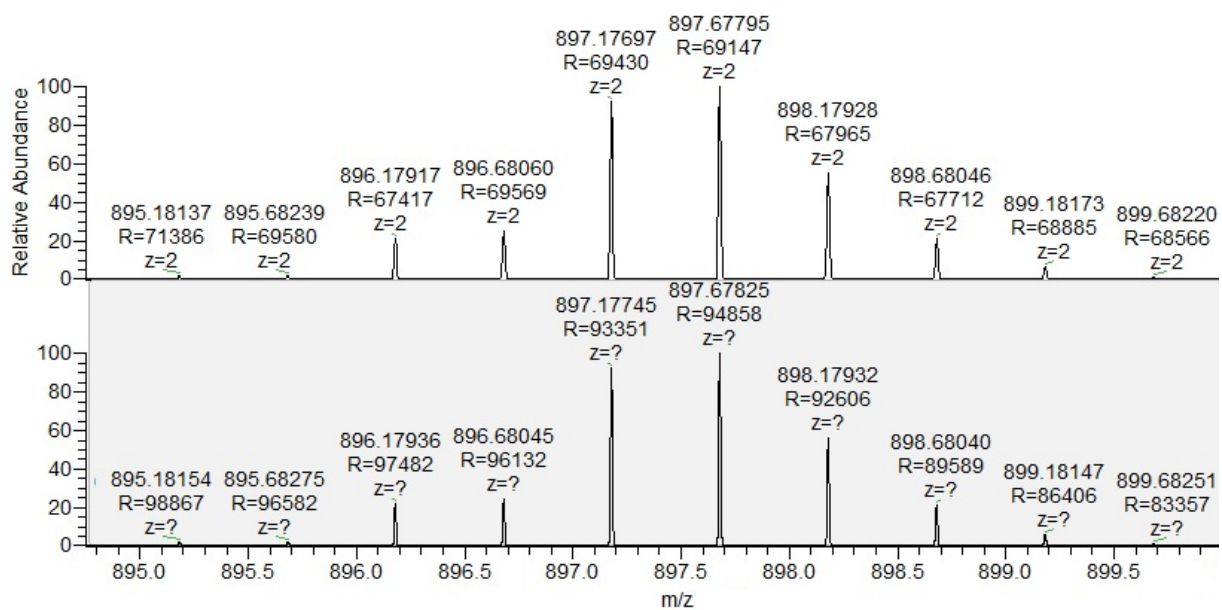


Figure S16. Mass spectrum of **Fe-8H** (top) and calculated isotope pattern for $[\text{Fe}_4(\text{HL})_2(\text{L})_2]^{2+}$ (bottom).

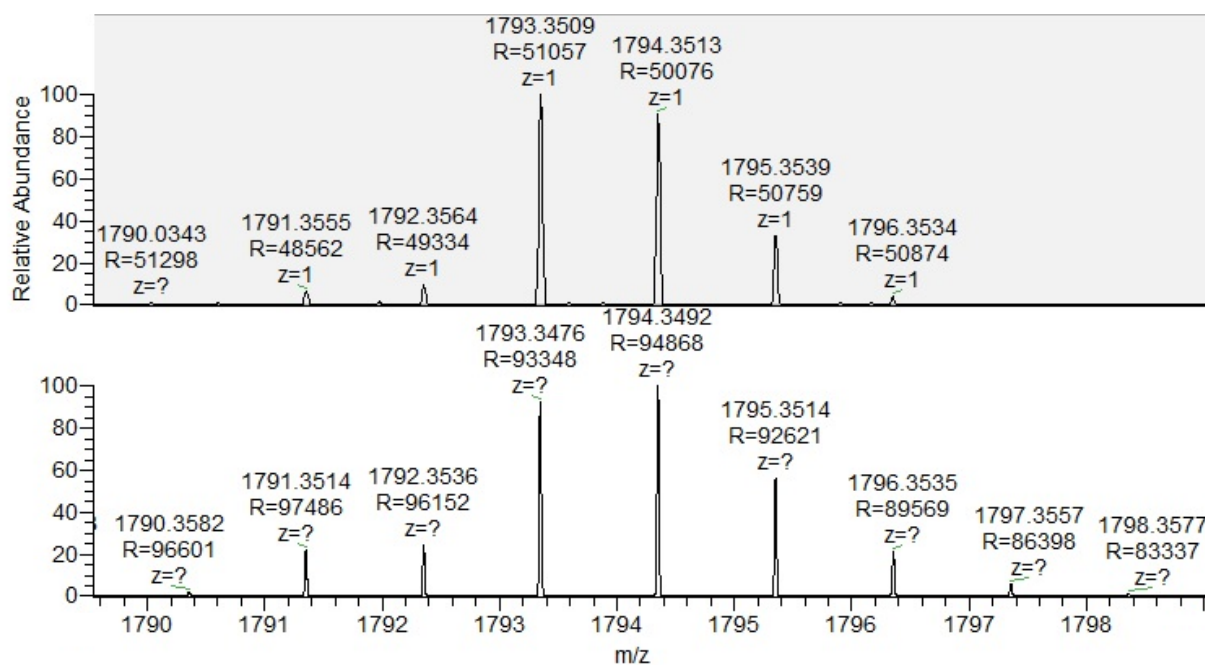


Figure S17. Mass spectrum of **Fe-8H** (top) and calculated isotope pattern for $[\text{Fe}_4(\text{HL})_1(\text{L})_3]^{1+}$ (bottom).

¹H and COSY NMR experiments

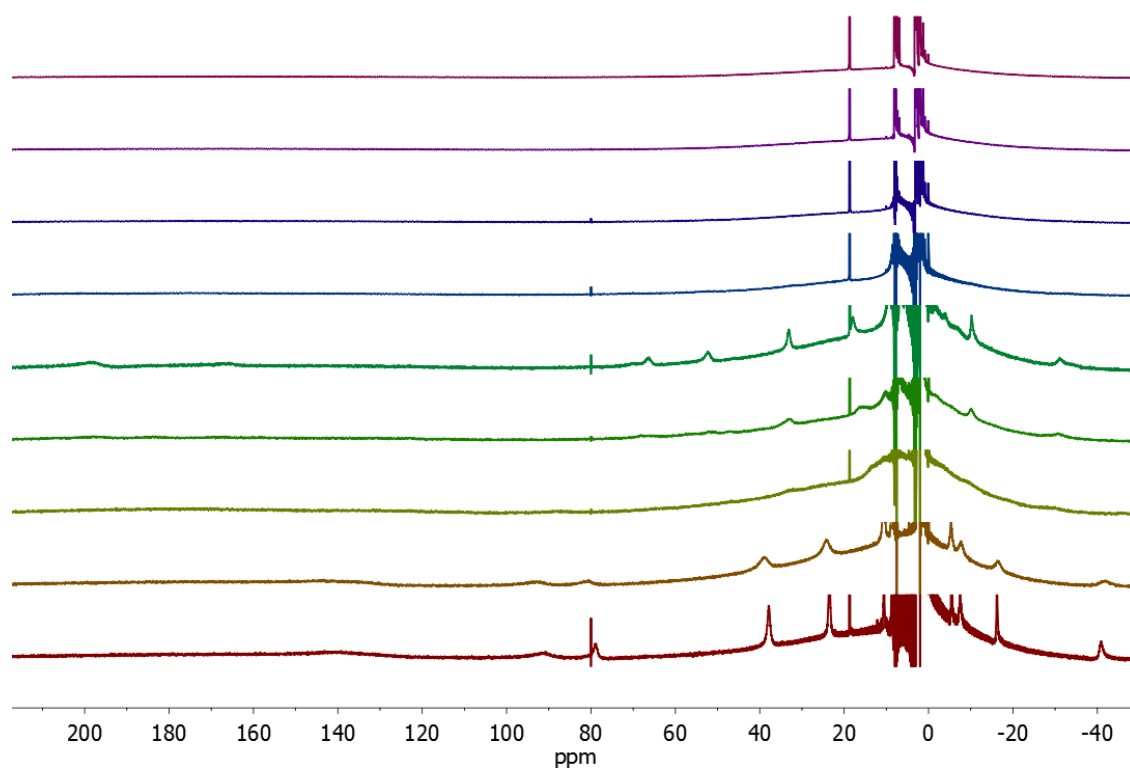


Figure S18. ¹H NMR titration spectra of **Fe-8H** with different equivalent of base (DMAN, 0 to 8 eq., bottom to top, respectively) in CD₃CN/CDCl₃ (1:1) at 25°C.

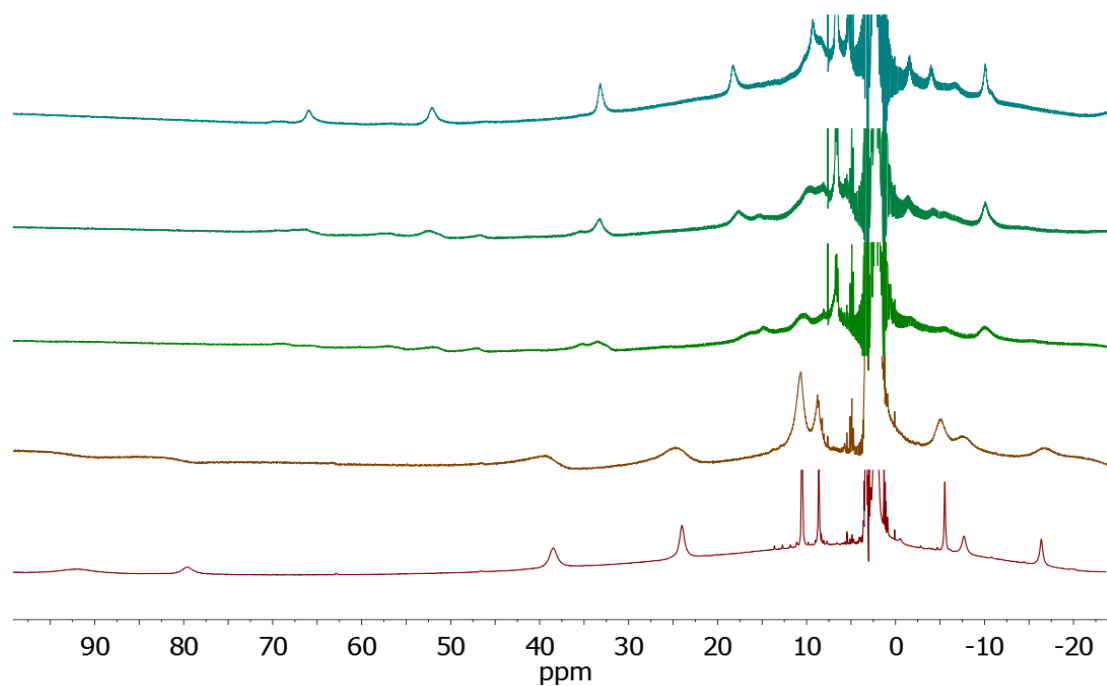


Figure S19. ¹H NMR titration spectra of **Fe-8H** with different equivalent of base (NEt₃, 0 to 4 eq., bottom to top, respectively) in CD₃CN at 25°C.

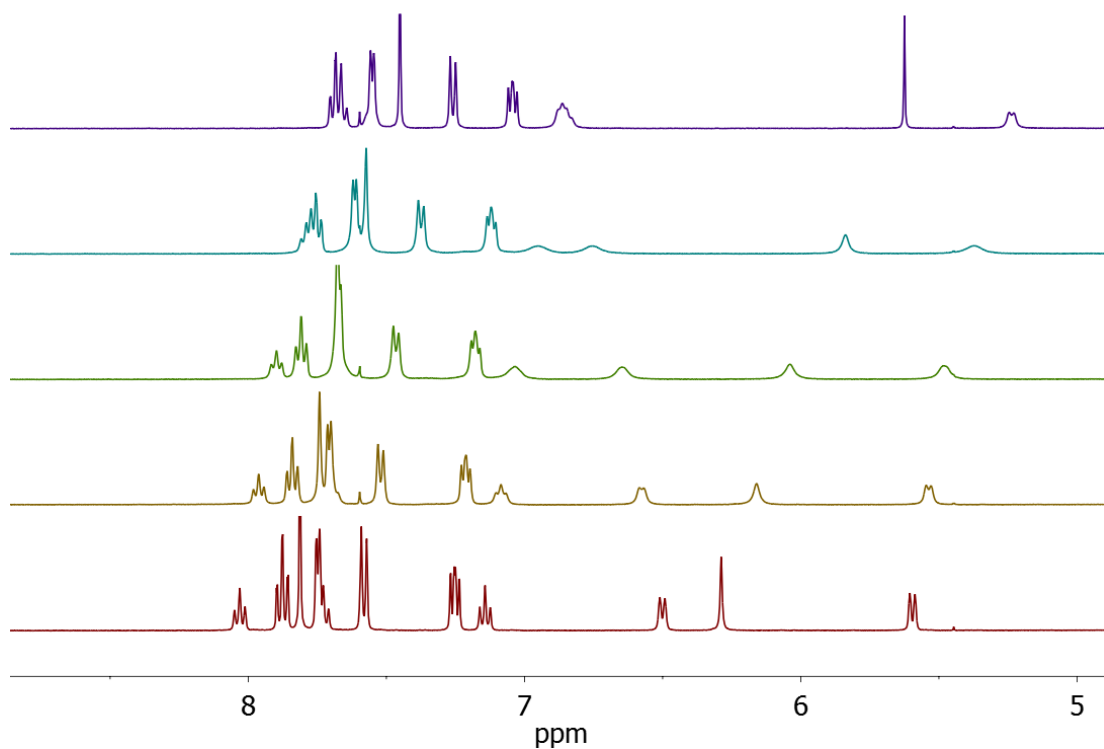


Figure S20. ^1H NMR titration spectra of **Zn-8H** with different equivalent of base (NEt_3 , 0 to 4 eq., bottom to top, respectively) in CD_3CN at 25°C .

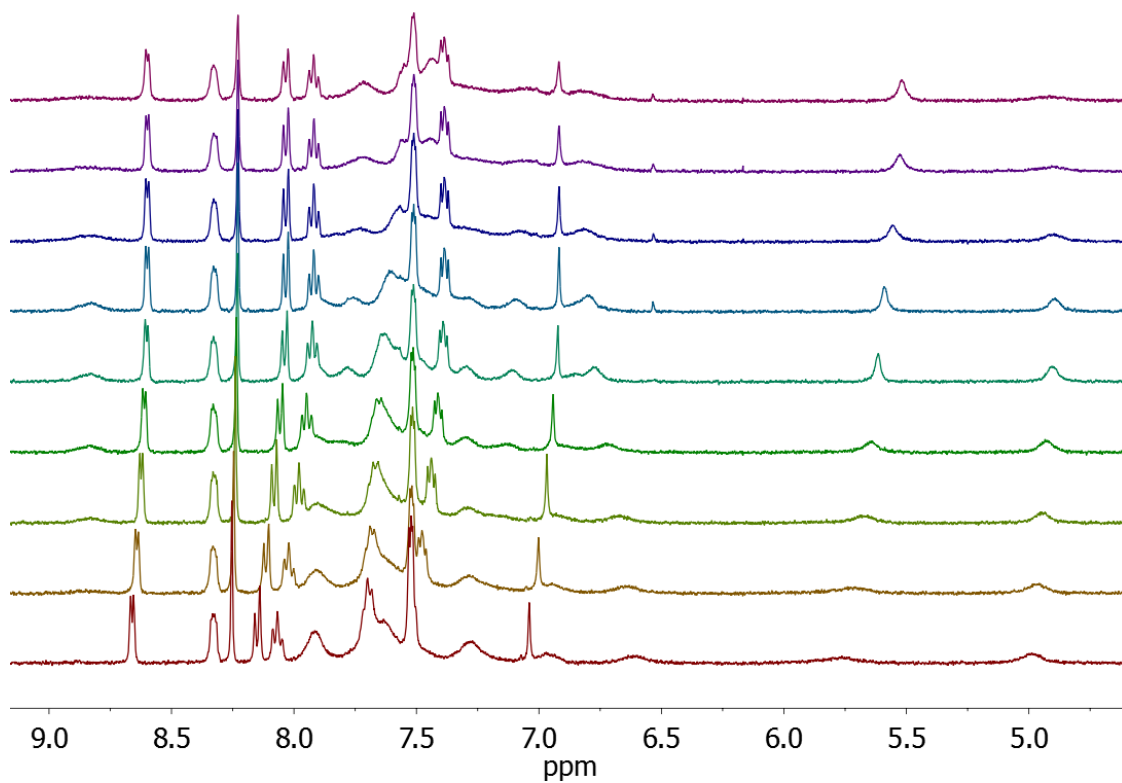


Figure S21. ^1H NMR titration spectra of **Zn-8H** with different equivalent of base (NEt_3 , 0 to 8 eq., bottom to top, respectively) in DMSO at 25°C .

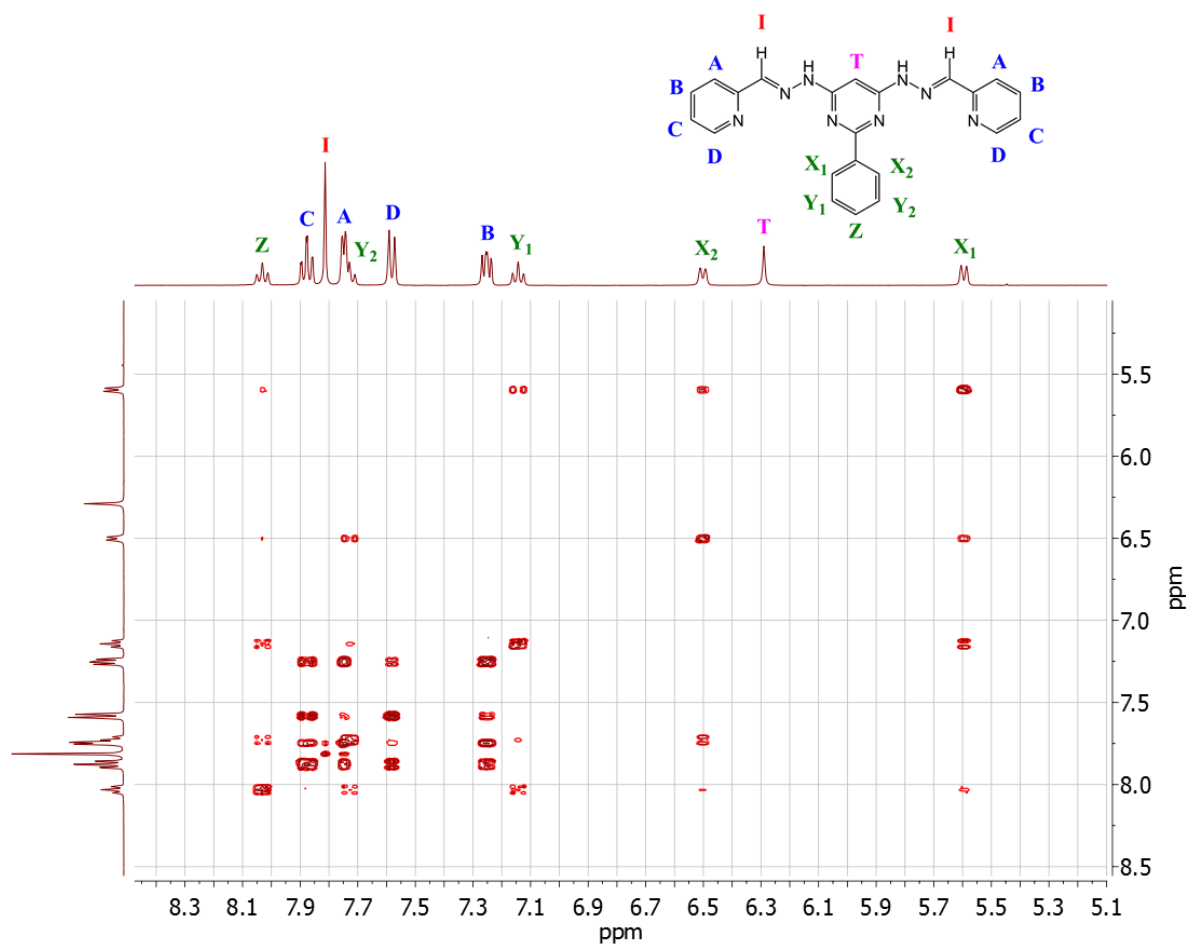


Figure S22. ¹H NMR COSY experiment for **Zn-8H** in CD₃CN at 25°C. A, B, C, D and I all integrate for 2 protons, as they are symmetrical. X₁ and X₂, as well as Y₁ and Y₂, have distinct chemical shifts due to the hindered rotation of the phenyl ring (see crystal structure of **Zn-8H**, Figure S7). Note that the NH proton cannot be seen as a result of fast exchange.

DFT calculations

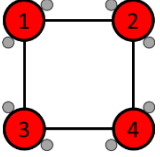
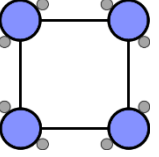
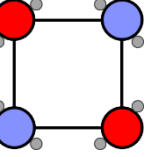
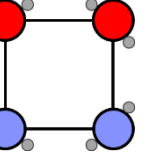
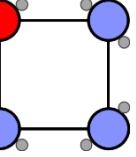
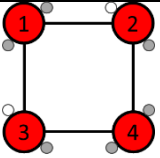
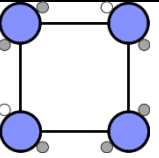
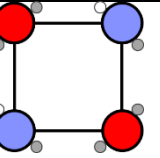
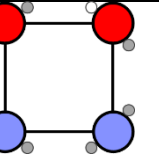
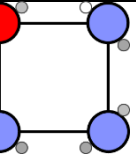
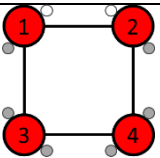
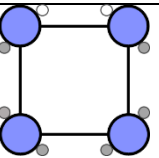
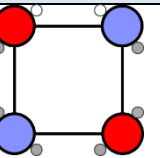
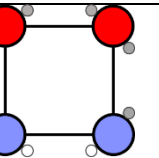
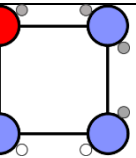
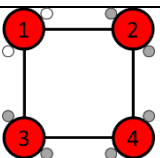
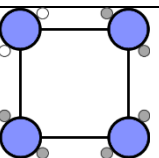
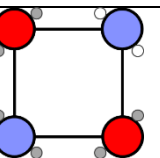
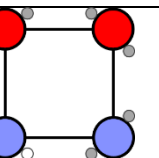
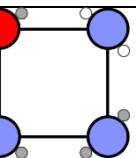
All H_{elec} were extracted from geometry optimizations of an isolated grid of four Fe centers, whose initial structure was taken from the reported unit cells. All calculations were carried out using Quantum Espresso (QE),^[9] the PBE functional with a Hubbard-like U parameter of 2.65 eV on the “ d ” orbitals of iron (PBE+ U), the D2 correction of Grimme,^[10] and Vanderbilt Ultrasoft pseudopotentials.^[11] The Makov-Payne correction has been used to deal with the charged grids in the unit cell.^[12] The use of a DFT-functional including the parameter U stems from the inability of neither GGA nor hybrid functionals to provide reliable values of H_{elec} . The former over-stabilize the LS state and the latter over-stabilize the HS state.^[13] The meta-hybrid functional TPSSH seems to be the best one at predicting spin-crossover characteristic temperatures and structures.^[14] However, despite being more expensive, its accuracy at computing H_{elec} is not better than PBE+ U provided that U is properly parametrized for the system of interest. In this case, the value $U = 2.65$ eV is adequate to describe H_{elec} in FeN₆-based compounds, since it describes correctly the relative ordering of the LS and HS states (*ie.* correct sign of ΔH_{elec}),^[15] it captures the trends measured experimentally (*ie.* correct change of ΔH_{elec}),^[16,17] and provides reasonable quantitative accuracy (*ie.* reasonable values of ΔH_{elec}) in comparison to other DFT functionals.

The pKa values were computed on isolated Fe centers (either HS or LS), in which the ligand is truncated at the bond between NH and the central pyrimidine. We have employed the free-enthalpy (G) in solution of the reaction (*ie.* direct method) as explained in the literature.^[18] Since we are interested in the first- and second- pKa values, we have computed the free-enthalpy of the protonated (Fe(H₂L)₂), mono-deprotonated (Fe(HL)H₂L) and bi-deprotonated (Fe(HL)₂) Fe sites. Those have been evaluated using the wB97XD functional, the 6-311++G(d,p) basis set and the $D2$ Grimme dispersion correction as implemented in Gaussian09.^[19] The solvent (acetonitrile) has been described implicitly (without using any explicit acetonitrile molecule) using the SMD method.^[20] This computational setup is the best at describing the pKa of small thiol molecules in water, yet a systematic overestimation of 8 pKa units has been reported without using explicit solvent molecules.^[18] In the absence of a better benchmark to rely upon, we adopted this setup in the present study. Even though the error is significant, the fact that it is systematic enables us to establish reliable trends of pKa₁ and pKa₂ values for the different Fe spin states.

Table S9. Electronic enthalpy, H_{elec} , values for relevant magnetic configurations and deprotonation patterns of **Fe-8H**, **Fe-6H**, **Fe-4H** and **Fe-3H**. Values are given *per molecule* and relative to the most stable state (with a blue background). The distribution of HS (red-filled circles) and LS (blue-filled circles) Fe centers, protons (grey small circles), and deprotonation sites (white small circles) within the grid is schematized on top.

Spin State	HS	LS	IS-trans	IS-cis	HLLL
Fe-8H					
H_{elec} (kJ/mol)	0.0	21.1	7.3	8.9	14.6
Fe-6H-Trans					
H_{elec} (kJ/mol)	6.5	4.2	0.0	4.4	1.7
Fe-6H-Cis					
H_{elec} (kJ/mol)	5.8	6.6	6.6	1.2	5.0
Fe-6H-Homo					
H_{elec} (kJ/mol)	17.2	13.5	8.7	7.9	11.6
Fe-4H-Hetero					
H_{elec} (kJ/mol)	38.2	16.2	27.1	28.2	21.8
Fe-4H-Homo					
H_{elec} (kJ/mol)	20.2	0.0	1.0	8.8	15.3
Spin State	HLLL	LS-Hetero	LS-Homo		
Fe-3H					
H_{elec} (kJ/mol)	1.3	8.0	0.0		

Table S10. Octahedricity parameters: $S(O_h)$ values^[7] as a measure of distortion of the Fe-N6 coordination sphere for the 1 to 4 SCO centers in all selected grids. The most stable states are indicated with a blue background.

Deprotonation		HS	LS	IS-trans	IS-cis	HLLL
Fe-8H						
$S(O_h)$	①	6.44	2.58	2.47	6.31	2.53
	②	6.51	2.60	6.36	6.40	2.53
	③	6.58	2.60	6.24	2.51	2.55
	④	6.46	2.58	2.47	2.48	6.38
	Avg.	6.50	2.59	4.39	4.43	3.50
Fe-6H-Trans						
$S(O_h)$	①	6.47	2.39	6.02	6.36	6.05
	②	6.77	2.41	2.33	6.08	2.37
	③	6.75	2.45	2.36	2.37	2.43
	④	6.46	2.42	5.95	2.41	2.38
	Avg.	6.61	2.42	4.17	4.30	3.31
Fe-6H-Cis						
$S(O_h)$	①	6.36	2.45	2.34	6.52	6.11
	②	7.07	2.45	6.07	6.30	2.33
	③	7.09	2.38	6.10	2.42	2.48
	④	6.50	2.40	2.29	2.48	2.46
	Avg.	6.76	2.42	4.20	4.43	3.34
Fe-6H-Homo						
$S(O_h)$	①	6.45	2.40	6.25	6.69	6.23
	②	6.58	2.42	2.32	6.20	2.38
	③	6.91	2.39	2.31	2.37	2.38
	④	6.48	2.40	6.23	2.37	2.36
	Avg.	6.61	2.40	4.28	4.41	3.33

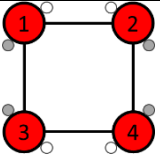
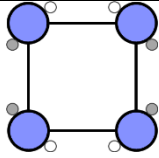
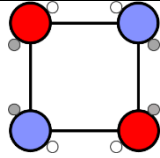
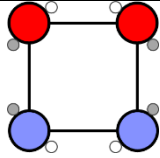
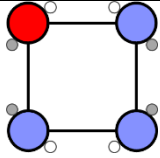
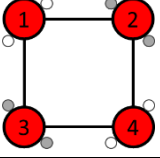
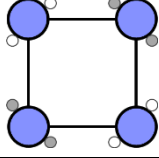
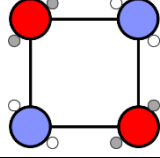
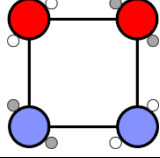
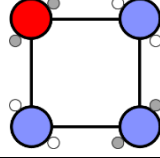
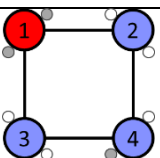
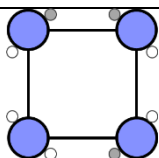
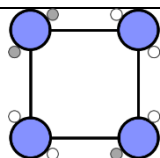
Fe-4H-Hetero						
$S(O_h)$	①	6.25	2.38	5.79	6.06	5.85
	②	6.83	2.42	2.34	5.96	2.33
	③	6.87	2.43	2.36	2.43	2.42
	④	6.24	2.43	6.03	2.39	2.41
	Avg.	6.55	2.41	4.13	4.21	3.25
Fe-4H-Homo						
$S(O_h)$	①	6.61	2.32	5.98	6.15	6.28
	②	6.58	2.41	2.37	6.15	2.35
	③	6.53	2.44	2.42	2.28	2.31
	④	6.62	2.28	6.19	2.35	2.40
	Avg.	6.58	2.36	4.24	4.23	3.34
Spin State		HLLL	LS-Hetero	LS-Homo		
Fe-3H						
$S(O_h)$	①	6.42	2.46	2.21		
	②	2.42	2.39	2.42		
	③	2.45	2.48	2.47		
	④	2.40	2.39	2.41		
	Avg.	3.42	2.43	2.38		

Table S11. Computed pKa1 and pKa2 values (at 25°C) of truncated Fe- and Zn-centers and of the isolated ligand.

	pKa ₁	pKa ₂
Fe(HS)	11.2	12.5
Fe(LS)	9.2	11.9
Zn	12.3	13.0
Ligand	22.5	26.7

References

- (1) (a) Sheldrick, G. M.; SADABS Version 2.03, Bruker Analytical X-Ray Systems, Madison, WI, USA, 2000. b) Sheldrick, G. M. *Acta Cryst. C71*, **2015**, 3. c) Spek, A. L. *Acta Cryst. C71*, **2015**, 9.
- (2) Gottlieb, H. E.; Kotlyar, V.; Nudelman, A. *J. Org. Chem.* **1997**, *62*, 7512.
- (3) Ruben, M.; Lehn, J.-M.; Vaughan, G. *Chem. Commun.* **2003**, 1338. (b) Uppadine, L. H.; Gisselbrecht, J.-P.; Lehn, J.-M. *Chem. Commun.* **2004**, 718. (c) Barboiu, M.; Ruben, M.; Blasen, G.; Kyritsakas, N.; Chacko, E.; Dutta, M.; Redekovich, O.; Leton, K.; Brook, D. J. R.; Lehn, J.-M. *Eur. J. Inorg. Chem.* **2006**, 784.
- (4) (a) Evans, D. F. *J. Chem. Soc.*, **1959**, 2003. (b) Lölinger, J.; Scheffold, R. *J. Chem. Educ.* **1972**, *49*, 646.
- (5) (a) Phillips, W. D.; Poe, M. *Meth. Enzymol.* **1972**, *24*, 304. (b) Schubert, E. M. *J. Chem. Educ.* **1992**, *69*, 62. (c) Live, D. H.; Chan, S. I. *Anal. Chem.* **1970**, *42*, 791.
- (6) Weast, R. C.; Astle, M. J.; Beyer, W. H. *CRC Handbook of Chemistry and Physics; 64 ed.*; CRC Press, **1983**.
- (7) Alvarez, S.; Avnir, D.; Llunell, M.; Pinsky, M. *New. J. Chem.* **2002**, *26*, 996.
- (8) Perrin, D. D.; Dempsey, B. *Buffers for pH and Metal Ion Control*, Chapman & Hall, London, **1984**.
- (9) Giannozzi, P.; Baroni, S.; Bonini, N.; Calandra, M.; Car, R.; Cavazzoni, C.; Ceresoli, D.; Chiarotti, G. L.; Cococcioni, M.; Dabo, I.; Corso, A. D.; Gironcoli, S. D.; Fabris, S.; Fratesi, G.; Gebauer, R.; Gerstmann, U.; Gougoussis, C.; Kokalj, A.; Lazzeri, M.; Martin-Samos, L.; Marzari, N.; Mauri, F.; Mazzarello, R.; Paolini, S.; Pasquarello, A.; Paulatto, L.; Sbraccia, C.; Scandolo, S.; Sclauzero, G.; Seitsonen, A. P.; Smogunov, A.; Umari, P.; Wentzcovitch, R. M. *J. Phys.: Condens. Matter* **2009**, *21*, 395502.
- (10) Grimme, S. *J. Comput. Chem.* **2006**, *27*, 1787.
- (11) Vanderbilt, D. *Phys. Rev. B* **1990**, *41*, 7892.
- (12) Makov, G.; Payne, M. *Phys. Rev. B* **1995**, *51*, 4014.
- (13) Lawson Daku, L. M.; Aquilante, F.; Robinson, T. W.; Hauser, A. *J. Chem. Theory Comput.* **2012**, *8*, 4216.
- (14) Cirera, J.; Paesani, F. *Inorg. Chem.* **2012**, *51*, 8194.
- (15) Vela, S.; Fumanal, M.; Ribas-Arino, J.; Robert, V. *Phys. Chem. Chem. Phys.* **2015**, *17*, 16306.
- (16) Vela, S.; Gourlaouen, C.; Fumanal, M.; Ribas-Arino, J. *Magnetochemistry* **2016**, *2*, 6.
- (17) Bartual-Murgui, C.; Vela, S.; Darawsheh, M.; Diego, R.; Teat, S. J.; Roubeau, O.; Aromi, G. *Inorg. Chem. Front.* **2017**, *4*, 1374.
- (18) Thapa, B.; Schlegel, H. B. *J. Phys. Chem. A* **2016**, *120*, 5726.

(19) Frisch, M. J.; Trucks, G. W.; Schlegel, H. B.; Scuseria, G. E.; Robb, M. A.; Cheeseman, J. R.; Scalmani, G.; Barone, V.; Mennucci, B.; Petersson, G. A.; Nakatsuji, H.; Caricato, M.; Li, X.; Hratchian, H. P.; Izmaylov, A. F.; Bloino, J.; Zheng, G.; Sonnenberg, J. L.; Hada, M.; Ehara, M.; Toyota, K.; Fukuda, R.; Hasegawa, J.; Ishida, M.; Nakajima, T.; Honda, Y.; Kitao, O.; Nakai, H.; Vreven, T.; Montgomery Jr., J. A.; Peralta, J. E.; Ogliaro, F.; Bearpark, M.; Heyd, J. J.; Brothers, E.; Kudin, K. N.; Staroverov, V. N.; Kobayashi, R.; Normand, J.; Raghavachari, K.; Rendell, A.; Burant, J. C.; Iyengar, S. S.; Tomasi, J.; Cossi, M.; Rega, N.; Millam, J. M.; Klene, M.; Knox, J. E.; Cross, J. B.; Bakken, V.; Adamo, C.; Jaramillo, J.; Gomperts, R.; Stratmann, R. E.; Yazyev, O.; Austin, A. J.; Cammi, R.; Pomelli, C.; Ochterski, J. W.; Martin, R. L.; Morokuma, K.; Zakrzewski, V. G.; Voth, G. A.; Salvador, P.; Dannenberg, J. J.; Dapprich, S.; Daniels, A. D.; Farkas, Ö.; Foresman, J. B.; Ortiz, J. V.; Cioslowski, J.; Fox, D. J. (Ed.: G. I. W. CT.), **2009**.

(20) Marenich, A. V.; Cramer, C. J.; Truhlar, D. G. *J. Phys. Chem. B* **2009**, *113*, 6378.